8-2020

Flexible Dye-Sensitized Solar Cells: a Study of Photoanode and Counter Electrode Materials

Brishty Deb Choudhury
The University of Texas Rio Grande Valley

FLEXIBLE DYE-SENSITIZED SOLAR CELLS: A STUDY OF PHOTOANODE AND COUNTER ELECTRODE MATERIALS

A Thesis

by

BRISHTY DEB CHOUDHURY

Submitted to the Graduate College of
The University of Texas Rio Grande Valley
In partial fulfillment of the requirements for the degree of

MASTER OF SCIENCE

August 2020

Major Subject: Chemistry

FLEXIBLE DYE-SENSITIZED SOLAR CELLS: A STUDY OF PHOTOANODE AND COUNTER ELECTRODE MATERIALS

A Thesis
by
BRISHTY DEB CHOUDHURY

COMMITTEE MEMBERS

Dr. Mohammed Jasim Uddin
Chair of Committee

Dr. Wei Lin
Committee Member

Dr. Karen Lozano
Committee Member

Dr. Hasina Huq
Committee Member

August 2020

ABSTRACT

Choudhury, Brishty Deb, Flexible Dye-Sensitized Solar Cells: A Study of Photoanode and Counter Electrode Materials. Master of Science (MS), August, 2020, 68 pp., 3 tables, 24 figures, references, 141 titles.

Compare to flat devices based on rigid substrates, fiber-shaped dye sensitized solar cells hold advantages of smaller size, light weight, facile fabrication, flexibility, and low cost, thus a promising direction for applications such as wearable electronic devices. Due to their unique photovoltaic properties, nanostructured morphologies of TiO_2 on flexible substrate have been studied extensively in the recent years for applications in dye sensitized solar cells (DSSCs). In the first part of this work the nano-tree morphology of the TiO_2 photoanode material on Ti wire has been investigated. To utilize the surface plasmon resonance (SPR) a plasmonic nanoparticle Ag has also been deposited using a very feasible photoreduction method. In the second part the micro-flower morphology of TiO_2 on Ti wire has been synthesized and structural and photoelectric performance has been evaluated. In the third part, a non-platinum catalyst for the counter electrode has been synthesized and a detailed study of the performance has been conducted.

DEDICATION

I deeply acknowledge my gratitude to my family and friends without whose support the completion of my master's degree would not have been possible. My Mother Gopa Datta Purkayastha, my father Shubhash Chandra Deyb Choudhury, and my friend Rajshakhar Paul inspired, motivated, and supported me throughout this journey to reach my goal. Thank you very much for your love and support.

ACKNOWLEDGEMENTS

I express my gratitude to Dr. Mohammed Jaism Uddin, chair of my dissertation committee, for providing me all the necessary support and guiding me throughout this journey. I want to thank Dr. Uddin for providing me all the instrumental and materialistic, and financial support, helping me editing my manuscripts, and encouraging to reach my goal with immense patience and positivity. I want to thank College of Science for providing me with the PGRA scholarship during the course of my MS study. My deep gratitude towards my committee members Dr. Wei Lin, Dr. Karen Lozano, Dr. Hasin Huq for providing their valuable time and evaluation of my research activities. I want to thank Dr. Karen Lozano and Dr. Hasina Huq for giving me their lab excess for scanning electron microscopy (SEM) analysis and magneton sputtering deposition, respectively. I want to thank the department chair Dr. B. Connie Allen, current and former graduate student coordinator Dr. Javier Macossay Torres, Dr. Evangelia Kotsikorou, Dr. Tulay A. Atesin for making my time in UTRGV great and pleasant.

I would like to express my deep gratitude to Dr. Chen Lin, who collaborated with me in my projects for giving me necessary training, insights, and inspiration to reach my goal. I would also like the thank Daniela Ramirez, Bernabe Ibarra, Javier Soliz-Martinez, the undergrads who worked with me in my projects. I want to thank my ex colleague Jared Jaksik for always being there for me to share his experience and insights regarding the research projects with me.

TABLE OF CONTENTS

Page

LIST OF TABLES

Page

LIST OF FIGURES

Page

CHAPTER I

INTRODUCTION

Rapid energy consumption and environmental pollution throughout modern times have created a global quest for clean and renewable alternative energy solutions, with many of the contenders ranging in wind, geothermal, biofuel, nuclear, solar, and many more. However, there are still many unknowns and safety precautions that are still to be studied. Wind energy, for example, is clean and arguably the most cost effective with a similar mechanism that has been used to power generators for decades, however they are rather noisy, intermittent on how windy the day is, and do require large amounts of open space and thus tend to be put out in open fields- the only places where human culture isn't jarring to nature. Geothermal energy revolves around using the earth's heat to power or generators, which is also reliable, useful for large scale installations, and saves up on costs, but at the same time are location dependent, and may cause surface instability and affect the environment around them in the long-run. Biofuel and Nuclear energy, though sustainable and relatively inexpensive, are still relatively new and due to the processes made to harness their energy, may lead to more harm than good in the long run. Solar energy on the other hand, is healthy, inexhaustible, and carries an untapped potential-possibly meeting mankind's exponentially increasing energy demands that when utilized properly can convert infinite solar energy to its true potential for our needs.

Solar energy is abundantly available across the earth with no combustion or harmful waste being produced in the process of harnessing, converting, and generating light and thermal

energy into electrical. the energy, it is clean and better yet, cheap. The sun, being the source and driving force of all life and living organisms (including us humans) on this planet and to a certain extent the rest of the solar system, however, only a small amount of that seemingly infinite energy gift-wrapped for us is used for generation of electrical power. Therefore it would be more convenient for both our sakes and the earths to find a way to harness solar energy to its greatest extent, namely through the use of photovoltaic cells, but at the time it is still challenging to achieve high photocatalytic and photoelectrochemical performances through solar light. This leads to some of the most promising methods to achieve the goal of plentiful efficient energy through the use of photovoltaic cells to harness and utilize sunlight to drive the internal chemical reactions that create electricity. Silicon-based solar devices are expensive due to their complicated production process, which limits this technology for urban and other commercial applications, but recently several thin film organic solar cells have been manufactured that enjoy a decisive advantage of lightweight, flexibility and low module cost over conventional silicon based solar modules. Among many types of photovoltaic cells currently being manufactured and experimented on, Dye-Sensitized solar cells (DSSCs), has garnered immense interest from researcher due their potential in low-cost power generation, environment friendly manufacturing and installation, ease of manufacturing, and relatively high photo-conversion efficiency.

In terms of cost effectiveness, optimum efficiency and easy fabrication, the dye-sensitized solar cell (DSSC) which is a subclass of thin film solar cells proved to be one of the most promising alternatives to the silicon solar cells. DSSC consists of different components i.e. substrate (conductive substrate or conductive film coated substrate), Semiconductor nanostructure (photoanode), sensitizer (dye), electrolyte and catalyst coated counter electrode. Each component in the DSSC contributes towards the photo current efficiency of the solar cell

and the good design of DSSC is always the optimization and trade-off between different components. The most important and major component of the DSSC is the choice of photoanode material and its structure which determines the current–voltage characteristics, i.e. open-circuit voltage (*Voc),* the photo-generated current density (*Jsc*), light scattering/absorption properties, dye pickup and the fill factor of the cell.

DSSCs typically consist of a nanocrystalline, in some cases a TiO_2 film, covered by a monolayer of dye molecules, electrolytes, and/or counter electrodes with a photoanode material that transports the injected electrons from the excited dye molecules to the external circuit and supports the sensitizer. The main issue with DSSCs made up of TiO_2 nanoparticles is the fact they suffer from large grain boundaries that may result in reduced electron transfer rates that may lower the performance. This can be fixed, however, by changing the morphology of TiO_2 photoanodes to achieve high performance by enhancing properties such as surface area, electron transport, electron-hole recombination rate and light harvesting features. One of the obstacles to producing more efficient DSSCs has been the fast charge recombination in the large surface area and grain boundaries between nanoparticles, trapping events.

To minimize the charge recombination in the photoanode of DSSCs, 1D (One-Dimensional) TiO_2 nanoparticles have been examined for their unique shape-dependent electronic and optical properties, as well as their accepted applications in a wide variety of electrochemical and photoelectrochemical devices and have been anticipated to give improved electron transport rates. Branching rutile arrays and hierarchical anatase nanowire arrays have been synthesized as well and applied in DSSCs, the conversion efficiency improving due to the enlarged surface area for dye adsorption. 1D nanostructured arrays extend vertically against the horizontal plane of the cell in front of the substrates to create structures that direct electron

transfer pathways, but are limited by their low internal surface area with fewer QDs loading, leading to both a low light harvesting and low electron collection efficiency. Some photogenerated pairs recombine quickly, which promote inefficiency in the photoinduced chemical reaction with a wide band gap and a fast recombination of photogenerated charge carriers to indicate the influence on the photoabsorption and photoactivity which may restrain activity under visible light. To improve on the design and performance of these cells, 3D array structures are implemented into 1D nanostructure backbones along a 2D (Two dimensional) nanosheets offering dimension. The TiO_2 nanotree arrays are then obtained on oxide substrates through a two-step hydrothermal method. The synthesized nanostructures are investigated by means of scanning and high-resolution transmission electron microscopy. Fully processed synthetic routes, such as hydrothermal or solvothermal protocols, have shown great promise and been used successfully to prepare 3D branched array structures while simultaneously accessing various precursors, solvents, and additives to control crystal growth. 3D hierarchical TiO_2 nanotree array structures have been successfully incorporated into a variety of photovoltaic devices as photoanodes, consistently displaying improved performance through a high surface area for sufficient sensitizer anchoring, fast electron transfer, and long electron lifetime for efficient charge collection, improved light absorption, and enhanced light harvesting between interlaced nano branches for efficient electrolyte filtration.

Due to their unique photovoltaic properties, nanostructured morphologies of TiO_2 on flexible substrate have been studied extensively in the recent years for applications in dye sensitized solar cells (DSSCs). Microstructured electrode materials with high surface area can facilitate rapid charge transport and thus improve the light-to-current conversion efficiency. Herein we present an improved photoanode with forest like photoactive TiO_2 hierarchical

microstructure using a simple and facile hydrothermal route. To utilize the surface plasmon resonance (SPR) and hence increase the photon conversion efficiency, a plasmonic nanoparticle Ag has also been deposited using a very feasible photoreduction method. The branched structure of the photoanode increases the dye loading by filling the space between the nanowires whereas Ag nanoparticles play the multiple roles of dye absorption and light scattering to increase the light-to-current conversion efficiency of the device. The branched structure provides a suitable matrix for the subsequent Ag deposition. They improve the charge collection efficiency by providing the preferential electron pathways. The high-density Ag nanoparticles deposited on the forest like structure also decrease the charge recombination and therefore improve the photovoltaic efficiency of the cells. As a result, the DSSC based on this novel photoanode shows remarkably higher photon conversion efficiency (η_{max}=4.0 % and η_{opt}=3.15 %) compared to the device based on pristine nanowire or forest-like TiO_2 structure. The flexibility of the device showed sustainable and efficient performance of the microcells. Also, we report an alkali hydrothermal method to prepare different TiO_2 structures on Ti wire. The morphology of samples was analyzed by scanning electron microscopy and revealed that this common strategy could not only form one-dimensional nanowires, but also two different types of flower-like TiO_2 hierarchical structures. The different structures could be achieved by carefully adjusting reaction parameters of the hydrothermal reaction. These structures were used as photoanodes to assemble fiber-shaped dye-sensitized solar cells, and the photoinduced photocurrent density-voltage curves were measured for these devices to show how these hierarchical flower-like TiO_2 structures affect photovoltaic properties compared to TiO_2 nanowire arrays.

The development of such a photoanode which can efficiently harvest the light with properties of increased dye pickup, light scattering ability, reduced recombination reaction and improved charge transport ability are the parameters to engineer for high conversion efficiency.

Platinum (Pt) counter electrodes (CEs) have consistently shown excellent electrocatalytic performance and hold the record of the highest power conversion efficiency (PCE) for dye-sensitized solar cells (DSSCs). However, its use for large-scale production is limited either by high temperature required for thermal decomposition of its precursor or by wastage of the material leading to high cost or sophisticated equipment. A novel photofabrication technique to fabricate highly transparent platinum counter electrodes by ultraviolet (UV) irradiation of platinic acid ($H_2PtCl_6.6H_2O$) on rigid fluorine-doped tin oxide (FTO) and flexible indium-doped tin oxide (ITO) on polyethylene terephthalate (PET) substrates is a facile and versatile method for the fabrication of Pt CEs for dye sensitized solar cells (DSSCs). The photo fabricated Pt CEs were used to fabricate bifacial DSSCs with power conversion efficiencies (PCEs) attaining 7.29% for front illumination and 5.85% for rear illumination. The highest percentage ratio of the rear illumination efficiency to the front illumination efficiency (ηR) of 85.92% was recorded while the least ηR is 77.91%. Highly electrocatalytic materials like platinum (Pt) are used to reduced I_3^- to I^- at the interface of the electrolyte/CE in order to sustain the flow of current and regenerate molecules of the oxidized sensitizer in the DSSCs devices.

A traditional DSSC is mainly composed of three parts, including a dye-sensitized nanocrystalline porous semiconductor photoanode, electrolyte and a Pt counter electrode. Although platinum can meet the main requirements of counter electrode material for DSSCs due to its high catalytic activity and good electrical conductivity, however, the high cost, limited reserve and the possibility of corroded by I_3^-/I^- redox electrolyte of Pt confine its application to

a large scale. Therefore, exploring non-platinum counter electrode material with low cost and high catalytic activity has important practical significance for large-scale application of DSSC. Carbonaceous material has long been regarded as the most popular candidate for substitution of Pt due to its high electrical conductivity, heat resistance, corrosion resistance, good catalytic activity and stability for the reduction of I_3^-, abundant reserves, low cost and so on. Carbon materials such as graphite, activated carbon, carbon black, carbon nanotube, carbon nanofiber and fullerene have been widely used as counter electrode materials. Since the discovery of graphene, it has been considered to be the most promising carbon material for the counter electrode material of DSSC. Because the special two-dimensional honeycomb crystal structure of graphene enables it with a series of excellent performances such as larger surface area, chemical stability, high transmittance and electrical conductivity.

Hence, it is important to develop alternative noble-metal-free materials that are capable of replacing platinum as electrocatalysts. The power conversion efficiency of DSSCs does not increase in proportion to an increase in the thickness of the platinum film, and it is possible to obtain a high-power conversion efficiency with a very thin platinum film of 2 nm. Such results suggest that production costs can be somewhat reduced by reducing the amount of platinum used. However, a more promising way to reduce the cost of DSSCs is to explore other low-costing materials that possess reasonably good catalytic activity. The general requirement of a photoelectrode material is that it should have a maximal optical function to absorb solar energy in the visible region with a high catalytic function. The electrocatalytic activity of the material can be improved by increasing the specific surface area, so the material must be prepared with nanoscale dimensions. This is because nanosized materials show different physical and chemical properties than bulk materials. In this review, the recent progress in the replacement of the

platinum counter electrode with other cheaper materials for DSSCs is presented. The platinum-free counter electrode materials are categorized into carbon materials, conducting polymers, inorganic metal oxides and metal sulfides, transition metal nitrides and carbides, and composite materials, and the advantages of these platinum-free catalysts for DSSCs are also highlighted.

Various efforts have been on in utilizing other non-platinum electrocatalytic materials as well as developing new technique for the fabrication of Pt CE1. Some of the alternative materials that have been investigated and reported include polymeric conducting materials such as poly(3,4-ethylenedioxy-thiophene):poly(styrenesulfonate), carbon materials, inorganic semiconducting chalcogenide compounds such as NiS, CoS, and CoSe, platonic composite materials, and other electrocatalytic composite materials. Polymeric conducting materials and carbon materials have the advantages of low costs, solution processing and low temperature fabrication requirement. However, Pt has consistently shown excellent electrocatalytic performance and holds the record of the highest PCE for DSSCs. Pt CEs are usually fabricated at an elevated temperature of 450 °C from platinic acid (H_2PtCl_6) precursor or vacuum sputtered from Pt target. Thermal decomposition of H_2PtCl_6 for the fabrication of Pt CE is not suitable for material with lower thermal stability at the required elevated temperature for the synthesis of Pt. Hence, flexible Pt CE on conductive polyethylene naphthalate (PEN), polyethylene terephthalate (PET) and textile cannot be achieved through thermal decomposition process. Sputtering deposition on the other hand results in wastage of material during deposition process, thereby, limiting its use for large scale production as it is not cost effective.

Researchers have reported several attempts at fabricating Pt CEs at low temperature. Electrodeposition technique is one of such methods employed in the fabrication of Pt CEs at low temperature. This method which takes place at room temperature involves three electrodes

configuration with transparent conductive oxide (TCO) substrate acting as the working electrode and electrolyte material containing platinic acid solution. A cyclic voltammetry process is then performed using an electrochemical system. Electrophoretic deposition was used. They prepared H_2PtCl_6 glycol solution and preheated it under stirring for 6 h in an atmosphere of argon. ITO-PEN substrates were immersed in the resulting Pt-colloid and driven by a D.C. field of 1.6 Vcm^{-1}. The Pt coated electrode was washed with deionized (DI) water and ethanol before being post thermally treated at 60 °C for 30 mins. Both electrodeposition and electrophoretic deposition methods have the shortcoming of large Pt loading in the electrochemical baths making them unfeasible for commercial production

Chemical wet-chemistry reduction has been utilized for the fabrication of Platinum (Pt) counter electrodes (CE), employing acidic reducing agents without subsequent treatment. Employing a chemical reduction method prepared in ethanol for the synthesis of nanostructured metallic Pt precursor is either spin-coated or drop coated on fluorine doped tin oxide (FTO) glass electrodes or indium doped tin oxide (ITO) PET flexible substrates and dried at room temperature. The coated surfaces were then treated with gaseous formic acid reducing agent at temperature of 100 °C for a period of 15 minutes.Using a modified chemical reduction method to fabricate Pt CEs. Polyvinylpyrrolidone (PVP) served as surfactant, $NaHBr_4$ as reducing agent, NaOH was used to achieve neutral platinic precursor and UV-ozone treatment was used to decompose the surfactant after deposition on FTO or ITO-PEN. Polyol reduction technique is a facile method of synthesis of Pt from H2PtCl6 whereby ethylene glycol (EG) is used as reducing agent. fabricated Pt CEs using EG solution of $H_2PtCl_6.6H_2O$. The deposited precursor was thermally treated at 180 °C. The synthesized Pt on the substrates exhibited dense and porous Pt structures. The earlier resulting from growth of Pt on the substrates following the reduction while

the latter is due to Pt nanoparticle precipitation used a similar polyol method with modification of the pH of the H_2PtCl_6 and preheating the precursor solution at 110 ℃ for 30 mins. They as well pretreated the substrates with 'piranha' and 3-mercaptopropyl(trimethoxysilane) (MPTMS) to produce a thiol-functionalized silane self- assembled monolayer (SAM) film on the conductive substrates. The as-prepared functionalized substrates were soaked in the platinic EG solution for 12 h and rinsed with ethanol to eliminate undesirable residues and dried in nitrogen environment. Currently, a lot of materials such as carbonaceous materials, transition metal compounds, conductive polymers, and hybrids have been explored to serve as counter electrodes. Among them, carbonaceous materials, including carbon black, graphite, activated carbon, graphene, carbon nanotubes, and carbon nanofibers, are promising candidates because of their low-cost, pleasurable catalytic activity, high electrical conductivity, and superior corrosion resistance. In particular, two-dimensional or one-dimensional carbon nanomaterials (graphene, CNTs and CNFs) with high surface area and favorable electron transfer capability have attracted growing attention. Compared to graphene and CNTs, CNFs prepared via electrospinning can be produced at low cost, simple preparation process, and high productivity. Therefore, CNFs exhibit promising potential for low-cost CE of DSSCs. Up to date, a few papers concerning CNFs based CE for DSSCs have been reported. Generally, they can be divided into three routes. One is improving the interconnection among CNFs and the adhesion between CNFs and FTO-glass substrate Another is controlling of the morphology and microstructure of CNFs. For example, prepared CNFs with hollow core highly mesoporous shell structure to improve surface area of CNFs, and hence a highly efficient DSSC was obtained. The third one is modification of CNFs through incorporation with carbon nano-mateirals (CNTs, graphene), metal or alloy nanoparticles (NPs) (Pt, Pd–Co, Fe–Ni), and transition metal compounds (TiC and WC).

Nevertheless, all these reports regarding the CNFs based CE are associated with glass based rigid DSSCs. As is well known, the DSSCs based on flexible substrates manifests lightweight and wide applications and can be fabricated with roll-to-roll or large-scale production. To achieve a flexible CE, CE materials are deposited on plastic substrates including ITO/polyethylene terephthalate (ITO/PET) or ITO/polyethylene naphthalate (ITO/PEN), and metal/polymer. The use of TCO increases the cost of DSSCs. Moreover, the adhesion between CE materials and TCO should be improved for a long-term stable CE. Accordingly, if the requirement for Pt- and TCO-free architecture and the use of a flexible substrate can be satisfied simultaneously, an extremely low-cost FDSSCs with potentially wide applications will be realized. Conductive polymers are expected to be promising flexible CEs because they can simultaneously act as CE materials and substrate due to their flexibility, transparency and high catalytic activity. However, complex fabrication process and poor stability limit their practical application. A flexible CNFs film can overcome these disadvantages. Compare to flat devices based on rigid substrates, fiber-shaped dye sensitized solar cells hold advantages of smaller size, light weight, facile fabrication, flexibility, and low cost, thus a promising direction for applications such as wearable electronic devices. However, most reported fiber-shaped dye sensitized solar cells use Pt wires as counter electrodes, which make the applications suffer from high cost and scarcity. Herein, a flexible Pt-free counter electrode is fabricated via depositing ternary nickel cobalt selenide (Ni-Co-Se) particles on the surface of carbon fibers. Scanning electron microscopy and X-Ray diffraction are used to characterize the counter electrode and alloy material. Results from bare and modified carbon fiber counter electrodes reveal that Ni-Co-Se alloy particles greatly enhance electrocatalytic activity and reduce the charge-transfer resistance, leading to tremendous improvement in power conversion efficiency, which is comparable with devices using Pt wire

counter electrode. Bending test is also performed to show the superior flexibility of the novel device.

CHAPTER II

REVIEW OF LITERATURE

Microstructure Photoanode with TiO_2 Nano-tree Array and Ag Nanoparticle

Global warming and climate changes are two of the major challenges that the present world is facing currently. Utilization of clean and renewable energy sources (i.e., solar, thermal, wind etc.) has long been an important research area to solve these issues since many decades. Solar energy is the most promising one among all the renewable energy sources due to its sustainable, abundant, and readily available nature. Over the past few decades researchers have put significant efforts to improve the performance and stability of the photovoltaic (PV) technologies such as dye sensitized, perovskite, and organic solar cells [1]. Currently the market for photovoltaic technology can be broadly divided into two types: 1) large module for terrestrial power supply, and 2) smaller modules for powering portable devices. Dye-sensitized solar cells (DSSC) can play an important contribution to both areas, and it has particularly promising potential in the second category [2]. The flexible dye-sensitized solar cells (FDSSC) has emerged as a revolutionary technology in past few years due to their ability to power portable and wearable electronics, especially in applications where flexibility is required [3].

Improving the efficiency of photovoltaic devices is always a critical focus in this field. For a DSSC or FDSSC, the component of critical importance is the dye/metal oxide interfaces. There

are various options for the metal oxide film (i.e., TiO_2, ZnO, SnO_2, etc.). One direction to achieve the goal of higher photon conversion efficiency falls in the development of this film with nanostructures that can result in larger surface area, thus increasing the amount of dye loading and improving light-harvesting property. The major disadvantage to use a nanomaterial with irregular structure as the metal oxide layer is the large number of surface traps, which leads to series of charge recombination, and slowdown the electron transfer rate [4, 5]. Therefore, researchers are particularly interested in adopting well aligned, one dimensional (1D) TiO_2 nanowire arrays (NWAs) for DSSCs [6-15]. In DSSC, the vertically grown TiO_2 NWAs on the surface of the conductive substrate provides straight conducting pathways, resulting faster charge transport, which is essential for effective charge collection [16-19]. However, one disadvantage of 1D TiO_2 nanowires is the low surface area because of free space between nanowires. Therefore, development of branched TiO_2 NWAs has been reported to increase the surface area [20-25]. For example, Shao et. al. reported that TiO_2 nanotree structure could help to increase the efficiency by ~25% to ~60% [20]. Sheng et. al. also demonstrated that DSSC based on branched TiO_2 NWAs showing surface area increasing by 71% and solar conversion efficiency increasing by 52%, compared to devices with unbranched NWAs [21].

Another way to fabricate devices with higher efficiency is to take use of surface plasmon resonance (SPR) from noble metal nanoparticles (NP) [26]. It is well known that when electromagnetic radiation shines on properly fabricated metal nanostructures, the oscillation of confined free electrons in the structure will be in resonance with the radiation, resulting in intense, highly localized electromagnetic fields. This phenomenon is called localized surface plasmon resonance (LSPR). Similar to other types of excitation, surface plasmons can decay via non-radiative pathway and transfer the energy collected from incident radiation to high-energy

electrons (hot electrons) [27-30]. Based on different carrier concentration, size and shape of the nanostructure, hot electrons generated from surface plasmons in Au and Ag nanoparticles can have different energies [31-33]. These hot electrons can be captured when the plasmonic nanostructure is accompanied with an appropriate n-type semiconductor, such as TiO_2, thus can be widely used in DSSCs. Compared to regular semiconductor-based devices, cells with plasmonic nanostructures are much less affected by the thermodynamic factors. It's comparatively easy to modify the size, shape and composition of the plasmonic nanostructures so that they can absorb wider range of solar spectrum. Besides, plasmonic nanostructures tend to have very strong absorption, which means a high light-trapping efficiency. Journals have been published showing that incorporating metal NPs, e.g. Au or Ag, on TiO_2 nanowire surfaces, enhance the light-to-current conversion efficiency [34-39]. For example, Liu et. al. incorporated Au nanoparticles in hierarchical TiO_2 nanorod arrays, and an increase of efficiency by 3.25% has been observed [36]. Hu et. al. reported Ag NPs synthesized via photo reducing $AgNO_3$ on branched TiO_2 nanorod arrays, and the DSSC with Ag NPs exhibits an efficiency improvement by > 50%, with respect to devices based on bare branched TiO_2 nanorods [39].

Though above-mentioned works show development in improving performance of DSSCs, most of them adopt sandwich-shaped flat cell design, i.e., the devices are assembled with the use of fluorine-doped tin oxide (FTO) glass. The rigid substrate forbids the application of DSSC where flexibility is needed. In order to solve this issue, several groups fabricated FDSSCs with TiO_2 nanostructures on more flexible substrates such as carbon fibers and Ti wires [3, 14, 15, 40, 41]. However, to the best of our knowledge, there is no report on adopting both directions (synthesis of hierarchical 1D nanostructure and depositing noble metal NPs) at the same time to improve the cell efficiency of FDSSC based on hierarchical TiO_2-nanostructures on Ti wire. In

this paper, we fabricated forest-like TiO_2 hierarchical nanowires on the surface of Ti wire via hydrothermal method. Ag nanoparticles were incorporated in this structure following a very facile photoreduction method [38]. In the SEM images, nanotree-like structures are observed, and Ag nanoparticles are decorated on these structures. Through photovoltaic characterization, we showed that the novel FDSSC devices fabricated based on this photoanode material have better performance than those with bare unbranched 1D TiO_2 NWAs, possibly because of the improved loading of dye molecule, light scattering, charge transport, and the SPR effect of the metal NPs. Bending test has been also conducted to show the flexibility of the device.

Novel Flower like TiO_2 Morphology for Photoanode

Titanium dioxide (TiO_2) is a widely used material in many different commercial areas such as paints, toothpaste, sunscreens, etc. [1-6], because it is stable, biologically and environmentally benign, inexpensive, and abundant in nature. Moreover, the excellent optical and electrical properties endowed TiO_2 extremely promising potential in photovoltaic applications [7-12]. Compare to other metal oxides, solar cells based on TiO_2 electrodes show highest stability in performance and largest energy conversion efficiency [9, 13-16].

However, TiO_2 possess two large disadvantages for applications in solar energy conversion: relatively poor charge transport property and wide bandgap. In fact, these two limitations can be overcome via engineering the materials to form nanostructures. It is well known that quantum confinement effects in nanomaterials can alter transport behaviors of charge carriers and shift the electronic band structure [17]. For example, in dye-sensitized solar cells (DSSCs), the key component is a photoanode typically consisting of mesoporous TiO_2 with dye

molecules adsorbed on it. It is believed that percolation in the TiO_2 nanoparticle network in traditional photoanodes causes loss of electrons thus limits device performance [18-21]. This major drawback can be solved by using highly ordered one-dimensional (1D) TiO_2 nanostructures, such as nanowires (NW) and nanotubes (NT), in photoanodes, as these structures can provide direct conducting pathways and reduce charge carrier recombination [22-24]. Therefore, it is crucial to control the nanostructures of TiO_2 to achieve appropriate size, morphology, crystalline phases, and specific surface area for diverse applications, because these parameters determine properties of TiO_2 nanomaterials [1, 25-29].

Among all TiO_2 nanomaterials, 1D nanostructures have unique properties, for example, confined electrons/photons transport and good mechanical properties, hence widely used not only in solar cells, but also in other applications such as batteries and photoelectrochemical cells for effective charge separation and collection [19, 30, 31]. Despite these advantages, 1D TiO_2 nanomaterials have relatively low surface area because of free space between individual nanostructure. Thus, researchers have worked to develop hierarchical TiO_2 nanostructures to solve this issue, such as flower-like TiO_2 structures. For example, Wang et. al. reported synthesis of TiO_2 flower-like nanostructures by Ti-H_2O_2 oxidation-hydrothermal method [32]. Hyam et. al. fabricated rutile TiO_2 nanoneedle flowers through electrochemical anodization in perchloric acid solution under room temperature [33]. In Xiang et. al.'s work, hierarchically flower-like TiO_2 superstructures with exposed {001} facets were obtained through solvothermal strategy using titanate nanotubes as precursor [34]. Xu et. al. showed preparation of flower-like TiO_2 particles using template-free solvothermal approach by using tetrabutyl tinanate (TBT) [35]. Zhao et. al. got 3D flower-like TiO_2 hierarchical microstructures by hydrothermal method using TBT and polyethylene pyrrole in acetic acid solution [36]. Li et. al. also reported flower-like TiO_2

nanostructures dominant with {001} facets, which were similar to those in [34], while they adopted a one-pot, template-free solvothermal method using TBT as Ti source without any precursors [37]. In Que et. al.'s article, flower-like structures with highly crystallized anatase TiO_2 nanosheets were synthesized through a one-pot hydrothermal process, using poly(-vinylpyrrolidone) (PVP), titanium isopropoxide (TTIP), and HF [38]. Zong et. al. reported 3D flower-like morphology of TiO_2 obtained by hydrothermal method with TTIP and acetic acid [39]. Liu et. al. demonstrated directly synthesis of flower-like TiO_2 crystals using TBT and ethylene glycol [40].

In the above-described studies, majority of them mainly focus on the photocatalytic properties of these unique hierarchical structures [32, 34, 39, 40]. In [33], [36] and [38], photovoltaic properties of TiO_2 flower-like structures were investigated, while all of them utilized sandwich-shaped flat cell design with conductive glasses. The rigidity of the devices forbids the application where flexibility is required. Besides, most of the TiO_2 hierarchical flower structures obtained were precipitated out in the reaction solution [33-40], no matter metallic Ti [33] or Ti-containing compounds [34-40] were commonly used as titanium source. If photovoltaic properties of these structures need to be investigated, extra steps are required for sample separation and purification, as well as deposition and stabilization of these materials on conductive substrates. These two problems can be easily solved by adopting the design of fiber-shaped dye sensitized solar cell (FDSSC) based on TiO_2 nanostructures directly grown on Ti wire. The surface of the Ti wire could be treated to obtain desired TiO_2 nanostructure, while the inner intact metal could behave as the conductive base for the photoanode. For example, Zhang et. al. used anodization method to obtain Ti NT arrays on Ti wires for FDSSC [41]; Liu et. al. synthesized Ti NW arrays on Ti wire via NaOH solution hydrothermal reaction [42]; Chu et. al.

report seeded growth of tree-like TiO_2 nanoarrays on Ti and other metal wires for FDSSC [43]. However, to our best knowledge, there is no report about direct fabrication of flower-like TiO_2 structures on Ti wire as the photoanode material for FDSSC. In this paper, we report fabrication of novel TiO_2 flower-like hierarchical structures on top of Ti wire via hydrothermal method in NaOH solution. In the SEM images, two different types of flower-like structures are well observed. Though photoelectric characterization, we show how the flower-like TiO_2 structures affect the photovoltaic property compared to 1D TiO_2 NW arrays.

Carbon Fiber Coated with Ni-Co-Se Alloy as the Counter Electrode

Energy is an essential utility in the society. However, as traditional sources of energy, fossil fuels (coal, crude oil, and natural gas) are known to have harmful effects on environments and human health. Therefore, development in renewable/clean energy sources (i.e., solar, thermal, wind, nuclear fusion, etc.) attracts most attention in the energy field by far and is a popular research area. Among all the renewable/clean energy sources, because of sustainability, abundancy, and readily availability in nature, solar energy is the most promising one. Therefore, tremendous efforts have been putting into this research area over the past few decades to improve photovoltaic (PV) technologies such as dye sensitized, perovskite, and organic solar cells [1]. Compare to other PV techniques, dye-sensitized solar cells (DSSCs) developed since late 1960s [2] have economic and simple fabrication processes and high power conversion efficiencies (PCEs) [3-5]. However, planar structure DSSCs using rigid substrates are not compatible with applications where super flexibility is required, e.g. wearable electronic device. Fiber-shaped DSSCs (FDSSCs) are one type of PV device molded into a flexible fibrous structure, and they

can be incorporated in broad rang of important applications due to smaller size, light weight, as well as ease in fabrication and low cost.

One general structure of a FDSSC has three major components: a photoanode, a counter electrode either arranged parallel to the photoanode or weaved around it, and an electrolyte with a pair of redox species. The most common photoanode consists dye molecules loaded on a layer of TiO_2, which is stable, biologically and environmentally benign, inexpensive, and has excellent optical and electrical properties [6-9]. TiO_2 based photoanode has been widely studied and used in FDSSCs, because its appropriate electronic band structures allow the photon-excited electrons from dye molecules (usu. N719) be injected into the TiO_2 layer. Then the electrons are conducted to an external circuit to generate electric power and finally reach the counter electrode. The photo-oxidized dye molecules after electron injection can be restored by accepting electrons from the electrolyte, usually an organic solvent containing I^-/I_3^- redox pair. The reduced species can be subsequently regenerated at the surface of counter electrode, by accepting the electron migrated through the external load. Overall, the device converts light energy to electric energy without permanently change the chemical composition of all components.

Though the photoanode plays the central role to generate electrons from light, the counter electrode is also critical in reforming the redox species. So far, many FDSSCs adopt Pt wire [10-15] or Pt based materials [16-17] as counter electrode, owing to high catalytic activity, chemical stability, and electrical conductivity [11, 18-22]. However, high cost and rarity of Pt forbids its large-scale industrialized application. Hence, scientists have been working on developing Pt-free counter electrodes for FDSSCs. Among all the materials investigated, carbon-based counter electrodes are considered ideal for fiber shaped devices, as they are highly conductive, mechanically robust, light weighted, low cost, and very flexible. On the other hand, major

shortcomings of carbon-based counter electrodes include slow charge transfer rate and limited ability for electrocatalysis of bare carbon materials. Researchers in this area have been working to solve these challenges. For example, L. Chen et. al. reported a FDSSC with TiO_2 nanotube arrays in the photoanode and bare carbon fiber (CF) as counter electrode had a power conversion efficiency (PCE) of 1.03%; when the bare CF was coated with $CoNi_2S_4$ nanorod or $CoNi_2S_4$ nanoribbon, PCE of devices dramatically improved to 4.10 % and 7.03%, respectively [23]. Z. Yang et. al. fabricated FDSSC with PCE 7.13%, and the counter electrode used was multiwall carbon nanotubes array (MWCNTs) [24]. In the work conducted by T. Chen et. al., the device had aligned titania nanotubes as photoanode material, and aligned carbon nanotubes (CNT) fibers in CE; the resulted PCE was 2.20% [25]. A. Ali et. al. showed that MWCNT coated with poly (3,4-ethylene dioxythiophene):poly(styrene sulfonate) reached PCE of 5.03% [26]. The highest PCE achieved by far based on Pt-free counter electrode (10.28%) was done by J. Zhang et. al.; their group used $Co_{0.85}Se$ nanosheets on the polyaniline functionalized CFs [27].

In the above-mentioned examples, higher PCE of the device could be achieved by coating a conductive polymer layer on the carbon-based counter electrode [26-27], and/or using transition metal chalcogenides [23, 27]. The latter method attracts attention because these materials are resistant to electrolyte corrosion, active for I_3^- reduction, and also inexpensive [28-29]. In L. Chen's article [23], ternary $CoNi_2S_4$ was used, as the device could take advantage of both cobalt and nickel ions, which could provide richer redox reactions than binary CoS or NiS. J. Zhang et. al. reported use of $Co_{0.85}Se$ [27], as metal selenides are known to have distinctive chemical and electronic properties, therefore great potential for broad range of applications [30-32]. In the work of L. Shao et. al. [33], hollow microspheres based on ternary nickel cobalt selenide (Ni-Co-Se) alloy were

synthesized via a simple one-step hydrothermal route, and the corresponding flat cell using this material in the CE had PCE up to 9.04% and higher than cells with Pt CE (8.07%).

In this work, we report synthesis of Ni-Co-Se particles, and the treatment on CF to incorporate the ternary metal selenides to form Pt-free fiber shaped CEs. Performances of devices with Ni-Co-Se synthesized at different temperatures, as well as FDSSCs with Pt CE, bare CF CE, and CF coated with Pt, are compared. The FDSSCs based on the Ni-Co-Se on carbon fiber (Ni-Co-Se@CF) counter electrode achieved a highest power conversion efficiency of 2.01%, comparable with CF CEs or CF CEs coated with Pt. Electrochemical characterization of CEs with Ni-Co-Se@CF shows inclusion of this alloy selenide has lower charge transfer resistance and better catalytic property than bare CF CEs. In addition, the fabricated FDSSCs show good flexibility.

CHAPTER III

METHODOLOGY AND FINDINGS

Microstructure Photoanode with TiO_2 Nano-tree Array and Ag Nanoparticles

Fabrication of TiO_2 NWAs: Several Ti wires (ϕ = 250 μm) were cleaned ultrasonically in ethanol and acetone for 15 minutes respectively. The treated wires were then put in a stainless steel autoclaves half filled with different concentrations of NaOH (i.e., 0.5 M, 1.5 M, 2.5 M, 5 M etc.) solutions. The sealed autoclaves were put in an electric furnace at 220°C for a period of 12 hours followed by natural cooling to room temperature. The treated nanowires are now covered with $Na_2Ti_2O_5 \cdot 3H_2O$ NWAs. These Ti wires were washed repeatedly with milli-Q water and acetone several times to remove the excess NaOH solution. The wires were then immersed in 1 M-2 M HCl acid solution for 1-2 hours where hydrogen ion (H^+) displacement occurs, and the sample converts to $H_2Ti_2O_4(OH)_2$ NWAs.

Fabrication of Nano-Tree Arrays (NTAs) and Decoration with Ag NPs: The as prepared wires were again transferred to stainless steel autoclaves filled with 25 mL of H_2SO_4 solutions (i.e., 0.015 M, 0.02 M, 0.025 M, and 0.03 M). The autoclaves were then put in an electric oven at

100°C for 4 hours. After that, the autoclaves were cooled down to room temperature and the wires were taken out of the autoclaves. The wires were washed repeatedly with milli-Q water and acetone to remove extra acid solution. Then wires were annealed at 500°C for 0.5 hours to obtain NTA with improved crystallinity. The as prepared NTA were then immersed into different concentrations (0.5 mM, 1 mM, 2 mM, etc.) of $AgNO_3$ for 5 mins and irradiated in UV-crosslinker for 30 mins to deposit Ag NPs. The wires are now ready to function as the photoanode.

Electrolyte Preparation: The electrolyte was prepared by dissolving 0.5 M LiI, 0.05 M I_2, and 0.5 M tert-butyl pyridine and brought up to 10 ml volume in 3-methoxy propionitrile. 5 wt% poly (vinylidene fluoride-co-hexafluoropropylene) was added to this solution and dissolved overnight with mild heating to make a homogeneous solution.

Fabrication of Fiber-Shaped Dye Sensitized Solar Cells: The as prepared photoanodes were immersed into a 0.5 mM N719 dye solution (solvent mixture of acetonitrile and tert-butyl alcohol in a volume ratio of 1:1) for 24 hours. After that, the photoanodes were washed repeatedly with acetonitrile to remove excess dye solution. A platinum wire (ϕ = 125μm) was twisted around the photoanode and the assembly was put into a transparent capillary tube. The electrolyte was injected into this capillary using a pipette.

Morphological and Photovoltaic Characterizations: The morphological characterization has been done using scanning electron microscopy (EVO LS10 STEM) equipped with EDS X-ray microanalyzer. The photocurrent-voltage measurements were carried out using a VersaSTAT3 potentiostat (Princeton Applied Research) running cyclic voltammetry with a scan rate of

50 mV· s^{-1}. A Honle solar simulator 400, with an AM 1.5G spectrum (100 mW/cm^2) was used to simulate sunlight for irradiating the cells.

Results and Discussion

Morphology Characterization

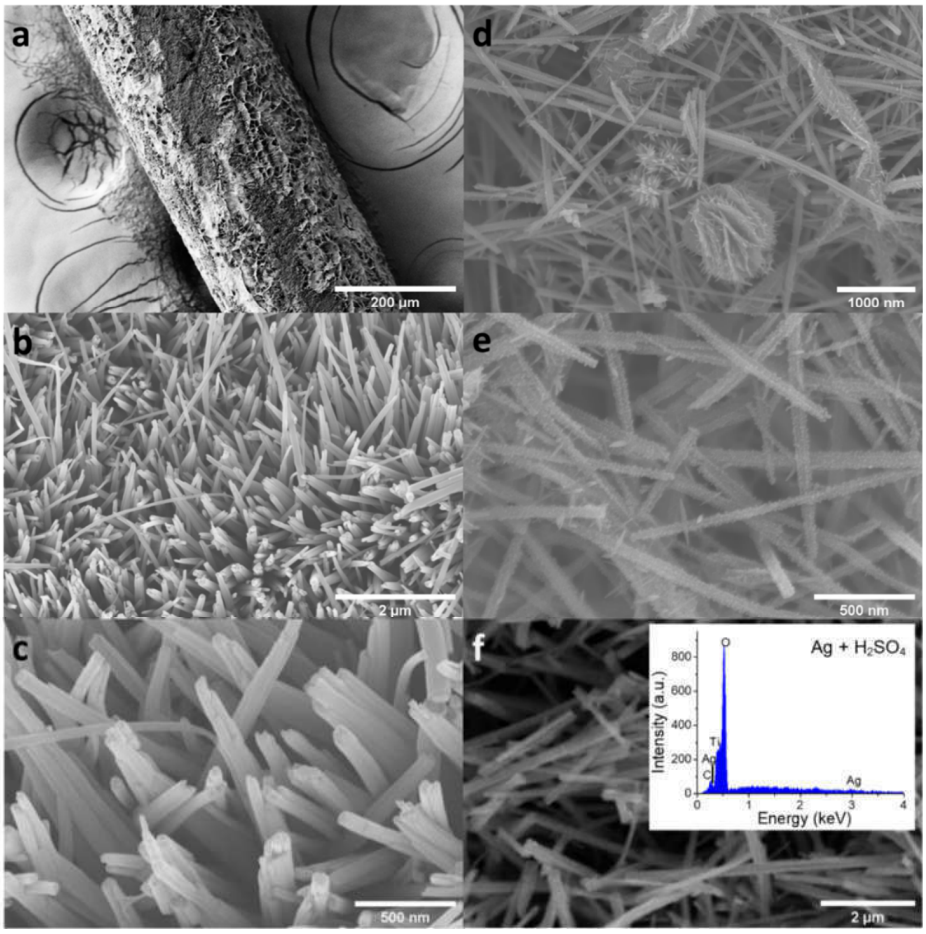

Figure 1: a) – c) SEM image of the Ti thread with TiO_2 NWAs at different magnifications; d) & e) Ti thread with TiO_2 NTA at different magnifications; f) SEM image of a particular region of the NTA film and corresponding EDS.

Fig 1 a) – c) shows an as-prepared Ti thread after coating with TiO_2. The rough surface from Fig 1 a) reveals the formation of the NWA growth over a larger area. The Ti thread becomes uniformly surrounded by the target material. The uniform distribution of the NWAs ensures that no metal surface is exposed and thus inhibits any possibility of short circuiting. Figs 1 b) and 1 c) shows the zoomed view of the NWA covered Ti wire at higher magnifications. It can be seen that the NWs are densely grown on the Ti substrate forming aligned arrays. It can be also seen that the NWs are grown vertically and then bended over each other to form a bridged structure. Although we did the photovoltaic performance evaluation of the photoanodes for different concentration of NaOH, a detailed morphological study with varying NaOH concentration has not been done in our investigation as they are already available in the literature [42, 43]. In our investigation, we found a concentration between 2 M to 3 M NaOH gives the best morphology. Various parameters play critical role for the successful deposition of the NWA film (i.e., number of Ti substrate in the hydrothermal reactor, length of the substrates, reaction time, cooling time, etc.). These parameters can significantly change the optimum NaOH concentration for a stable NWA morphology. The reason can be explained by the fact that the number of Ti substrate and their length can significantly control the source of Ti wire as well as the potential site for the nanowire growth. The reaction time also plays a similar role. In our investigation for NTA growth, we found an optimum concentration of 2.5 M NaOH gives a stable film morphology capable for branched growth. However, a higher NaOH concentration more than 3 M always resulted into cracked film for our experimental condition, coming out of the substrate exposing bare metals at spots and thus proving the potential site for short circuiting. Fig 1 d) and 1 e) shows individual nanobranches at higher magnifications. Numerous sharp niddle-like

morphologies with clean and smooth surfaces are clearly visible on the individual nanowires. Based on the top view of the SEM images, the niddle like structures has a length ranging from 19.831 nm to 47.854 nm. However, it is very interesting that how the different in H_2SO_4 concentration significantly affects the morphology of the nanostrucres. We have treated the nanowires with a range of H_2SO_4 concentrations (i.e., 0.015 M, 0.02 M, 0.025 M, 0.03 M, etc.), and found that an acid concentration of 0.02 M – 0.025 M favors formation of niddle like nanobranches as can be seen in Fig 1 d) and 1 e). After further increasing the acid concentration, nanowires are found broken into small pieces and aggregates into lumps. Fig 1 f) shows a particular region of the NTA film and the inset shows the corresponding EDS spectra. A clear SEM image of Ag NPs on the nanobranches has not been possible to obtain mainly because of the sputtering of gold- palladium (Au-Pd) NPs on them. The EDS result confirms the formation of TiO_2 and deposition of Ag NPs.

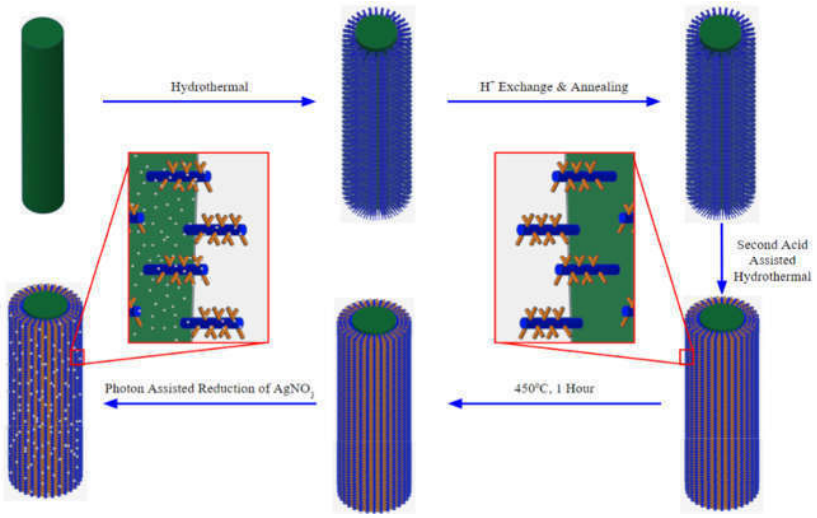

Figure 2**:** Schematic growth mechanism of the Novel Hierarchical Photoanode

Formation Mechanism of NWAs and NTAs

A set of reaction condition was used to determine the formation mechanism of the NWA and NTA. The time for hydrothermal reaction in NaOH solution was varied between 6 hours to 24 hours. Also, the acid assisted hydrothermal reaction was done directly on the $Na_2Ti_2O_5 \cdot 3H_2O$ NWAs and then the H^+ ion displacement was performed. In case of both NWAs and NTAs, an extended hydrothermal reaction time resulted into the destruction of the films and becoming dispersed powders in the solution. Based on our observations and previous studies we can assume the formation mechanism to be dissolution-recrystallization process [42, 44, 45]. The proposed mechanism for NTA growth can be described as follows. The Ti wire acts both as the substrate and source of Ti and reacts with NaOH to form $Na_2Ti_2O_5 \cdot 3H_2O$ nanocrystals via hydrothermal reaction. The diffusion of Ti atom from the inside of the wire to the surface initiates the reaction and proceeds with time. The resultant $Na_2Ti_2O_5 \cdot 3H_2O$ nanocrystals act as the nuclei for the subsequent growth of the $Na_2Ti_2O_5 \cdot 3H_2O$ NWA. Treating of these NWAs with HCl results into exchange of Na^+ with H^+ and forms $H_2Ti_2O_4(OH)_2$ NWA. These $H_2Ti_2O_4(OH)_2$ NWA reacts with H_2SO_4 according to the following reaction:

$$H_2SO_4 + H_2Ti_2O_4(OH)_2 \rightarrow Ti(SO_4)_2 + H_2O$$

$Ti(SO_4)_2$ then undergoes hydrolysis to produce TiO_2 nanoparticles which eventually get deposited on to the $H_2Ti_2O_4(OH)_2$ NWA.

$$Ti(SO_4)_2 + H_2O \rightarrow TiO_2 + H_2SO_4$$

The success of the process depends on the surface of the NWA which plays a duel role by providing both the Ti source and locations for crystal growth. Another important parameter is the reaction time. With increasing reaction time, the TiO_2 nanocrystals gradually forms a dendritic structures which eventually transforms into monocrystals [44].

Photovoltaic Characterizations

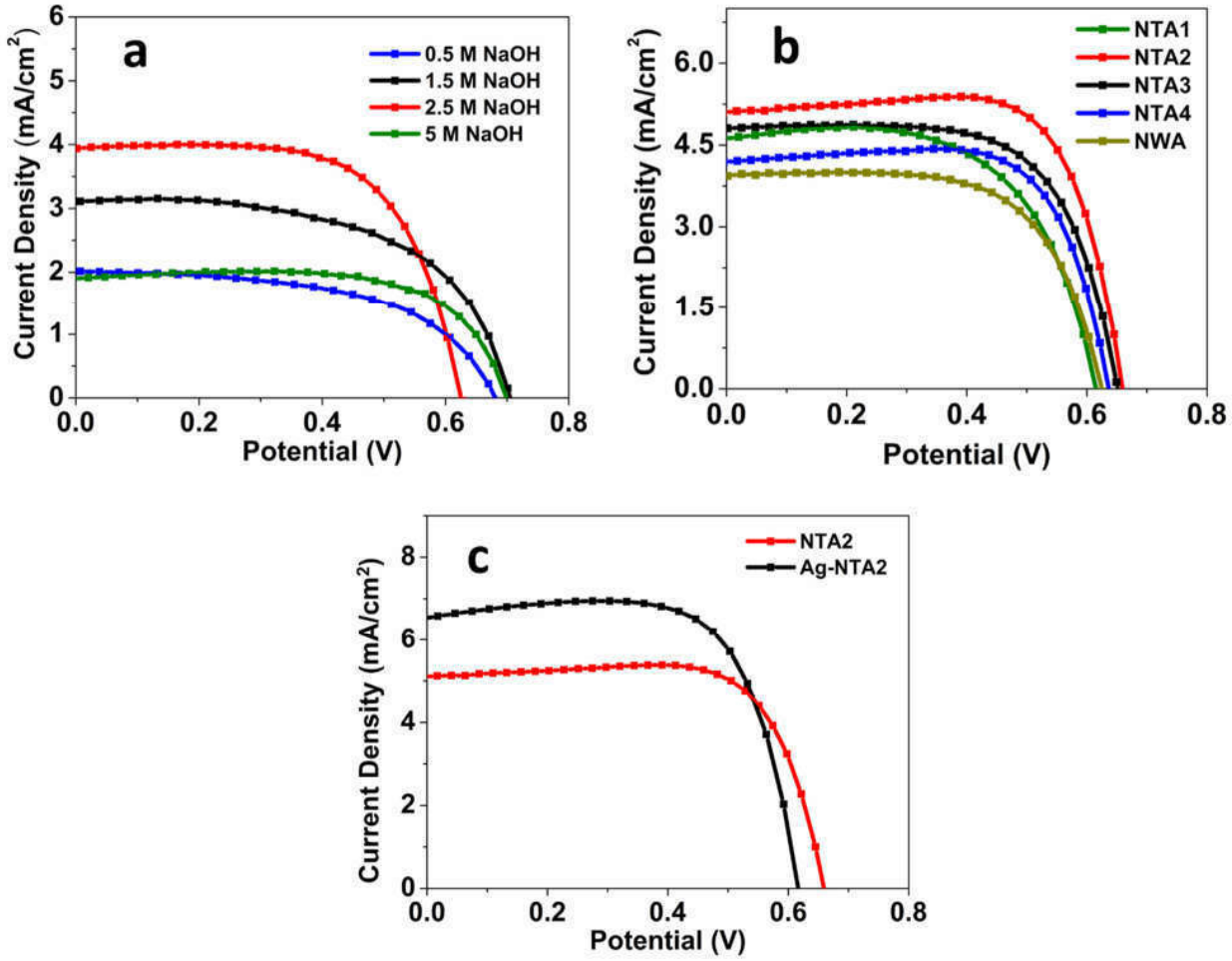

Figure 3: a) Optimization of base concentration; b) Optimization of H_2SO_4 for the NTA; **c)** Comparison of nano-tree TiO_2 and Ag deposited nano-tree TiO_2.

Fig 3 a) shows the optimization of NaOH concentration for obtaining best performance device under a specific set of experimental conditions. The concentration of NaOH solution has a significant contribution on the length of the NWA which subsequently affects the light-to-current conversion efficiency. In the past studies it has been found that, the electron diffusion length in

the one dimensional (1D) nanostructures is approximately 100 μm [46, 47]. However, in case of TiO_2 nanowire the diffusion length is 10.4 μm [48]. The internal surface area and amount of dye absorption increases as a function of nanowire length. As a result, the performance of the solar cell also increases with increasing concentration as can been seen from Fig 3 a). As the concentration increases form 0.5 M to 2.5 M the efficiency of the cell increases from 0.762% to 1.64% corresponding to a 115.22% increase. Increased NaOH concentration not only increases the length of the nanowire but also makes a thicker film. As a result, the amount of dye absorbed also increases [42]. However, an excessively high NaOH concentration, on the contrary, decreases the efficiency significantly as can be seen in the line for 5 M NaOH concentration. The efficiency drops abruptly to 0.974%. With increasing NaOH concentration and hydrothermal reaction time, a continuous film is created at the surface of the Ti substrate by the fusion of the nanowires at their roots due to the increased thickness [49]. As a result of the increased diameter and fusion of the nanowires, the effective internal surface area available for sensitized trapping is lost, which results in a decreased light-to-current efficiency [50]. The increased diameter and resulting film reduce the distance that an electron can travel after being injected to the conduction band (CB). When this distance is less than the diffusion length of the nanowire, recombination of the photogenerated electron and hole happens resulting in the poor performance of the solar cell. With increasing concentration, the NWA film cracks due to the week contact with the Ti substrate and becomes dispersed powder and thus again reduces the effective internal surface area available. Another important limitation that arises due to the increased NaOH concentration and subsequent increase in nanowire length is the reduced transmittance of the incident light [51, 52]. As the nanowire length increases it blocks the incident light to pass through the inner length and excite the absorbed sensitizer. As a result, the

efficiency decreases. However, surface area of TiO_2 nanowires is still insufficient compared to the other morphologies (i.e., nanoparticles, nanotubes, etc.). To increase the surface area and subsequently dye loading Fig 3 b) shows the H_2SO_4 corrosion treatment of the nanowires to obtain nano-tree morphology. From the study of Fig 3 a) the optimum concentration of 2.5 M has been found to be the most efficient under the given set of experimental conditions. A set of acid concentrations (i.e., 0.015 M, 0.02 M, 0.025 M, 0.03 M) has been used to treat the surface of the nanowires to form branches. The name of the photoanodes has been assigned NTA1, NTA2, NTA3, NTA4. Compared with the NWA solar cell, NTA2 gives an 128.08% increase in the efficiency. This increased efficiency can be attributed to the additional branches that creates more surface area available for the dye absorption. The enhanced light scattering, trapping, fast electron transport offered by the side branches also plays a significant role to increase the short-circuit current density (J_{sc}) and efficiency (η) in case of NTA2. The branched structure also allows good penetration of the electrolyte improving the electrode/electrolyte interfacial contact which in turn improves the fill factor (FF) [53]. The nano-branches also contributes to the improved efficiency by effectively transporting the photoinjected electron from the dye to the electrode. A faster electron transport improves the charge collection efficiency which in turn improves the short circuit current density from 3.86 mA/cm^2 to 5.05 mA/cm^2. The branched structure also provides larger diffusion length and thus inhibits recombination of the photogenerated electrons to holes in the electrolyte. However, as the acid concentration is increased further to 0.025 M, a slight reduction of performance is observed. An increase in acid concentration to 0.03 M significantly decreases the efficiency by 71.0%. The reason can be attributed to the fact that, at higher acid concentration the nanowires break into individual pieces, probably due to the corrosion of the nanowires. The broken pieces aggregates together to either

form lumps or become randomly oriented pieces on the film. The effective surface area reduces significantly, and the potential charge trapping sites also increases. This ultimately leads to low charge collection efficiency and hence the poor performance of the device.

Table 1: Photovoltaic performance of DSSC based on various photoanodes at standard condition.

Photoanode	J_{sc}, mA/cm^2	V_{oc}, Volt	Efficiency, %	FF
NWA	3.86	0.625	1.64	0.68
NTA1	4.63	0.620	1.82	0.64
NTA2	5.05	0.660	2.55	0.77
NTA3	4.75	0.650	2.12	0.69
NTA4	4.18	0.630	1.99	0.75
Ag-NTA4	6.53	0.620	2.96	0.734

Table 2: Best photovoltaic performance of DSSC based on various photoanodes, figure provided in the supporting information (SI).

Photoanode	J_{sc}, mA/cm^2	V_{oc}, Volt	Efficiency, %	FF
NWA	2.85	0.713	1.46	0.72
NTA1	4.85	1.03	2.51	0.50
NTA2	5.66	1.11	3.33	0.53

NTA3	5.41	0.890	3.01	0.63
NTA4	2.15	0.730	1.00	0.64
Ag-NTA4	6.41	0.882	4.02	0.71

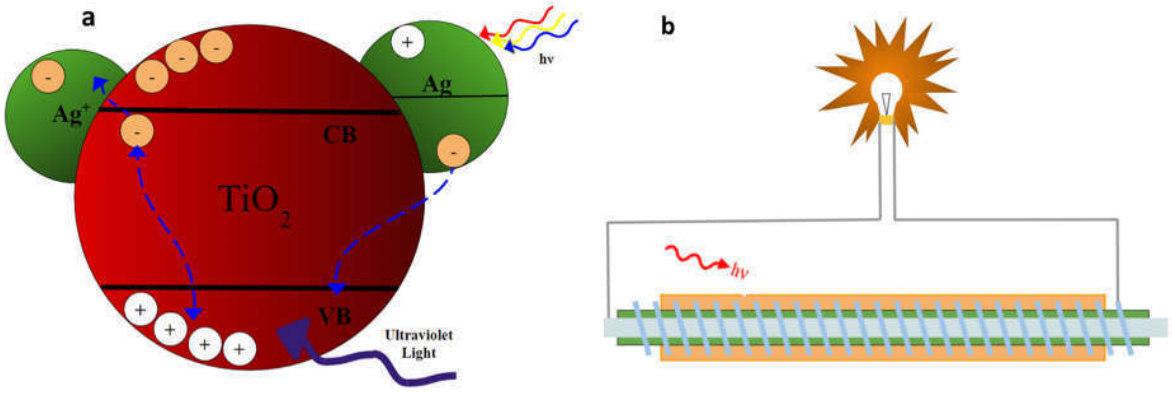

Figure 4: Optoelectronic band diagram of Ag/TiO_2 heterojunction

To further increase the efficiency, silver nanoparticles were deposited on the NTA to utilize the surface plasmonic resonance (SPR). Fig 3 c) shows the comparison between bare NTA based solar cell device and Ag deposited NTA based solar cell device. After depositing the Ag-NPs the short circuit current density increases significantly from 5.05 mA/cm^2 to 5.98 mA/cm^2. As a result, a 18.4% increase in the light-to-current conversion efficiency has been observed. The higher performance can be attributed to the reduced recombination of electron-hole pairs due to the Ag-TiO_2 junction. In the presence of Ag-NPs the absorption range of TiO_2 NTAs extends in

the wavelength region of 400-500 nm due to the SPR. As a result, the charge carrier concentration increases greatly. When the visible light hits the surface of the Ag-NPs, the photogenerated electrons from the fermi level of Ag jumps to the valance band (VB) of TiO_2. In the presence of Ultra-violet irradiation, the photogenerated electron from the VB of TiO_2 transfers to the conduction band (CB) of the TiO_2. The enhanced electromagnetic field that is produced in the presence of Ag-NPs improves light absorption of dye molecules and thus excites more electron than usual [54]. Ag-NPs also improves the light scattering due to the large plasmonic size [31]. A Schottky barrier is established at the Ag/TiO_2 junction due to the large work function of Ag. This barrier creates an electric field which promotes the efficient separation of the photogenerated electrons and holes. As a result, the electrons can efficiently travel through the branches and reach the electrode while the hole travels to the electrolyte and get captured by the reduced species [55]. Another way to explain the role of Ag-NPs is through the energy levels of the photoanode materials. Under irradiation the lower unoccupied molecular orbital (LUMO) of dye molecule contains photogenerated electrons which can then move to both Ag-NPs and the CB of the TiO_2 simultaneously. Due to the upcoming electrons, the Fermi level of the Ag shifts towards more negative potential until it comes closer to the Fermi level of the TiO_2. The electron in the Ag-NPs then move to the CB of TiO_2 due to the SPR effect while the Schottky barrier at the Ag/TiO_2 junction inhibits the backward diffusion of electron to the dye or electrolyte. As a result, the recombination of electrons and holes is significantly reduced, and the efficiency is increased [56].

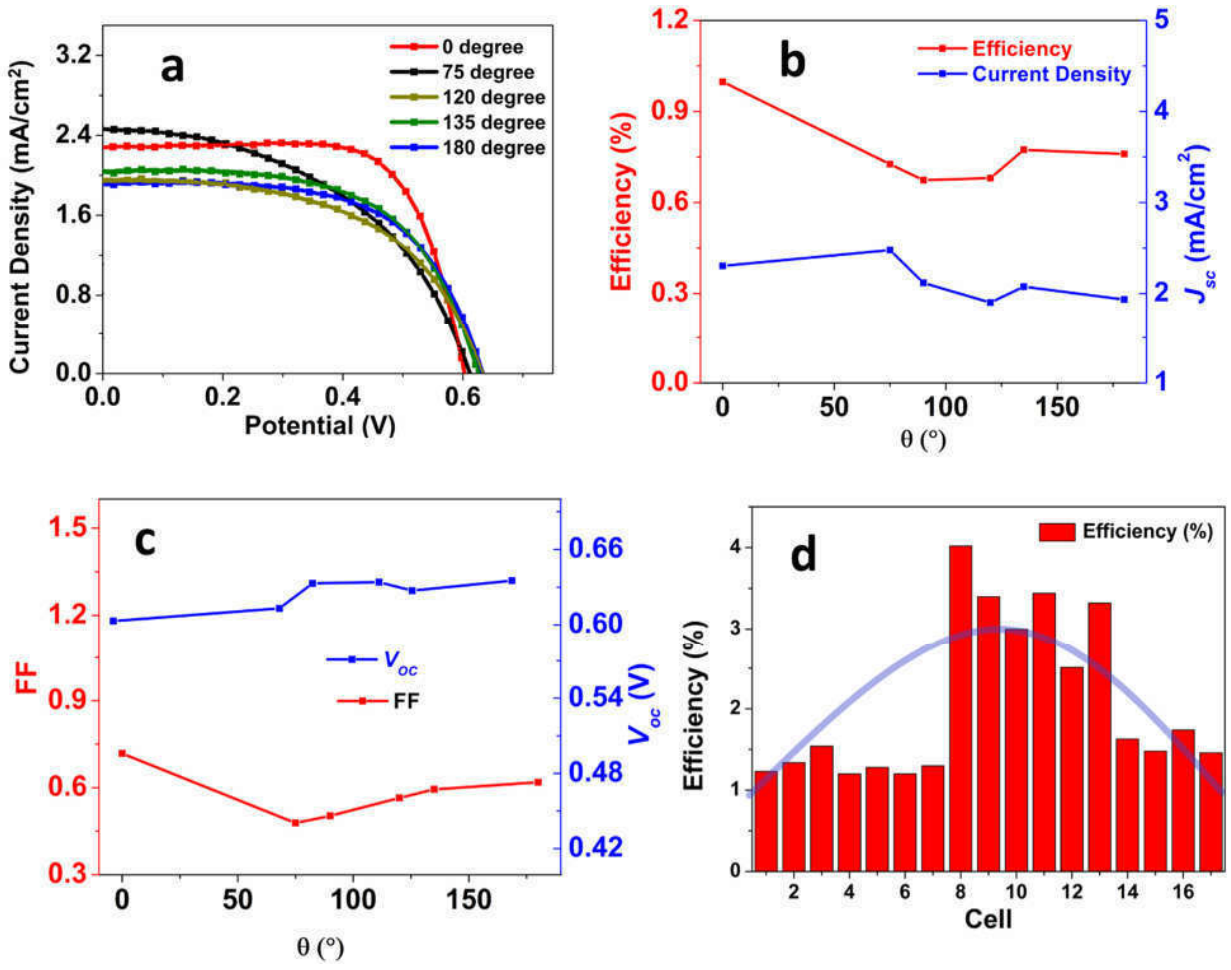

Figure 5: a) The flexibility test of the cells; b) Variation of η and J_{sc} with bending angle; c) Variation of FF and V_{oc} with bending angle; d) Efficiency variation of 18 cells.

To test the applicability of the device, various test has been performed. Fig 5 a) shows the I-V plot of the cells when they are bent at certain angles. There are a few parameters which can affect the performance of a solar cell during the bending test: 1) Electrical property degradation of the Ti wire substrate, 2) electrocatalytic property degradation of the Pt counter electrode, 3) leak of electrolyte, and 4) failure of the TiO_2 NWAs. It has been found that the efficiency drops only by 28.0% when the bending angle is 75°, making the device suitable for applications that

requires flexibility. After that, the efficiency does not vary much as the bending angle is increased further. When the bending angle the 180°, the decrease in efficiency is 25%, which is very similar to the initial drop in the performance. The initial drop in efficiency can be explained by above mentioned parameters. However, in actual experiment no significant leakage of the electrolyte has been found. Past studies have shown that the electrocatalytic performance of platinum counter electrode is not affected by repeated bending [57]. As the resistance of Ti substrate does not change significantly upon bending, the reason for poor performance can be attributed to the failure of the TiO_2 NTA film. TiO_2 NTA film cracks and falls off upon repeated bending and thus the efficiency of the device drops initially. Fig 5 b) shows the relation of efficiency and J_{sc} with the bending angle. Both J_{sc} and efficiency shows a very weak dependence on bending angle. As the cell is bent initially to 75° the almost no change is observed in *Jsc*. The trend is retained until a bending angle of 180°. However, efficiency only decreases slightly when the bending angle is 75° and then does not vary much with the bending angle. As already mentioned, failure of the NTA film is the major reason for the decreased performance. Fig 5 c) shows the behavior of FF and V_{oc} with bending angle. The FF initially decreases by 33.8% and then keeps increasing slightly with the bending angle although. This treand is very understandable from the I-V plot (Fig 5-a), which shows that the maximum power point initially decreases and then increases with bending angle and thus affecting the FF. When the cell is bent initially a disruption is introduced in the nanoscale environment which probably lowers the maximum power point. However, with time the disruption stabilizes, and the FF also increased subsequently. The *Voc* stays almost same with the bending angle, which proves that the cell resistance is very stable and does not disrupt charge transport upon bending, which again explains why after initial bending to 75° angle the *Jsc* value does not change significantly. Fig 5

d) shows the bar diagram of the efficiency of 18 cells. While most cells have efficiencies close to ~1.5%, a significant number of them has efficiency higher than 2.5% with the highest efficiency being 4.02%. A thorough investigation can be done on the individual parameters (length of the substrate, reaction time, connection to the electrode, etc.) to obtain a more consistent trend. With improved connectivity and proper execution of each reaction step it is very much possible to get efficiency significantly higher than 4%.

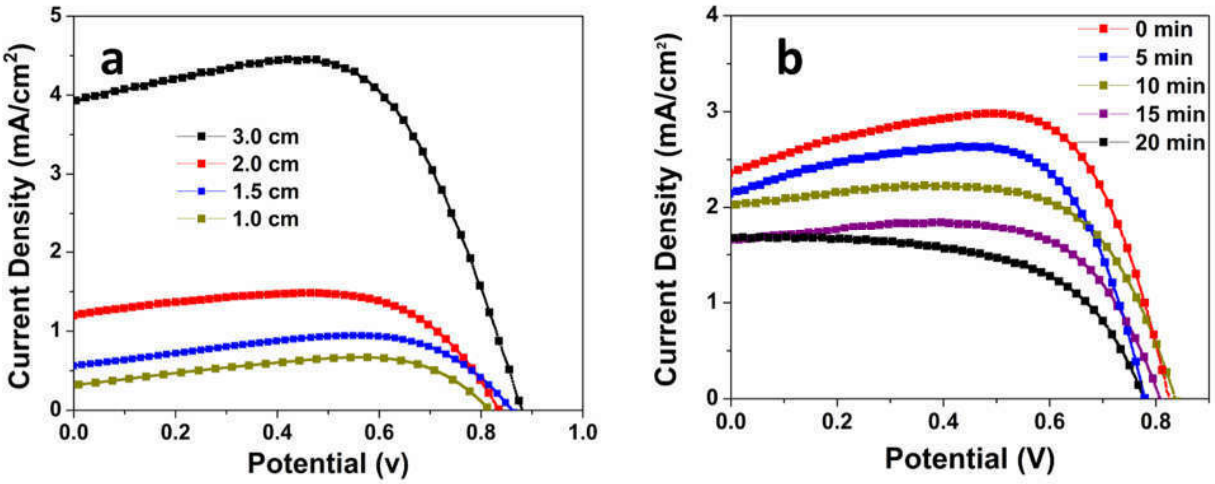

Figure 6: a) Comparison of photovoltaic performance with increasing length; **b)** Comparison of performance in cold ambient temperature.

Fig 6 a) shows the effect of cell length on the performance of the device. As expected with increasing length, the performance of the device increases significantly, making it a promising technology for large scale industrial applications and wearable and portable electronics. The efficiency increases from 0.37% to 2.45% when the cell length is increased from 1.0 cm to 3.0 cm. The increased surface area, higher dye loading, potential site for reduction, and

light scattering are the reasons for the higher performance at increasing length. Fig 6 b) shows the effect of cold temperature in the performance of the device. All the three parameters, short circuit current density J_{sc}, open circuit voltage V_{oc}, and efficiency decreases with decreasing temperatures which is very understandable from the fact that, charge transport increases at higher temperature and decreases at lower temperature. However, the cell still works at a reasonable efficiency at lower temperature making it suitable for applications requiring diverse operational temperatures.

Novel Flower like TiO_2 Morphology for Photoanode

Experiments

Fabrication of TiO_2 Nanostructures: Several Ti wires (ϕ = 250 μm) were cleaned ultrasonically in ethanol and acetone for 15 minutes subsequently to remove any impurities. The treated wires were then put in 30 mL of 2.5 M NaOH aqueous solution in 50 mL Teflon-lined stainless-steel autoclaves. The sealed autoclaves were put in an electric furnace at 220°C for various times (6 h, 9 h, 12 h, 24 h) followed by natural cooling to room temperature. Then these Ti wires were washed repeatedly with milli-Q water several times to remove the excess NaOH solution. After that, samples were immersed in 1 M HCl solution for 1 h to replace Na^+ with H^+. Finally, the as-prepared samples were calcined at 500°C for 30 min. Moreover, effects of reaction temperature were also studied by varying oven temperature from 180°C to 240°C.

Fabrication of Fiber-Shaped Dye Sensitized Solar Cells: The as prepared photoanodes were immersed into a 0.5 mM N719 dye solution (solvent mixture of acetonitrile and tert-butyl alcohol in a volume ratio of 1:1) for 24 hours. After that, the photoanodes were washed repeatedly with acetonitrile to remove excess dye solution. A platinum wire (ϕ = 125μm) was

aligned parallel to the photoanode in a transparent capillary tube. The electrolyte was injected into this capillary using a pipette. The electrolyte was prepared by dissolving 0.5 M LiI, 0.05 M I_2, and 0.5 M tert-butyl pyridine and brought up to 10 ml volume in 3-methoxy propionitrile. 5 wt% poly (vinylidene fluoride-co-hexafluoropropylene) was added to this solution and dissolved overnight with mild heating to make a homogeneous solution.

Morphological and Photovoltaic Characterizations: The morphological characterization has been done using scanning electron microscopy (EVO LS10 STEM). The photocurrent-voltage measurements were carried out using a VersaSTAT3 potentiostat (Princeton Applied Research) running cyclic voltammetry with a scan rate of 50 $mV \cdot s^{-1}$. A Honle solar simulator 400, with an AM 1.5G spectrum (100 mW/cm^2) was used to simulate sunlight for irradiating the cells.

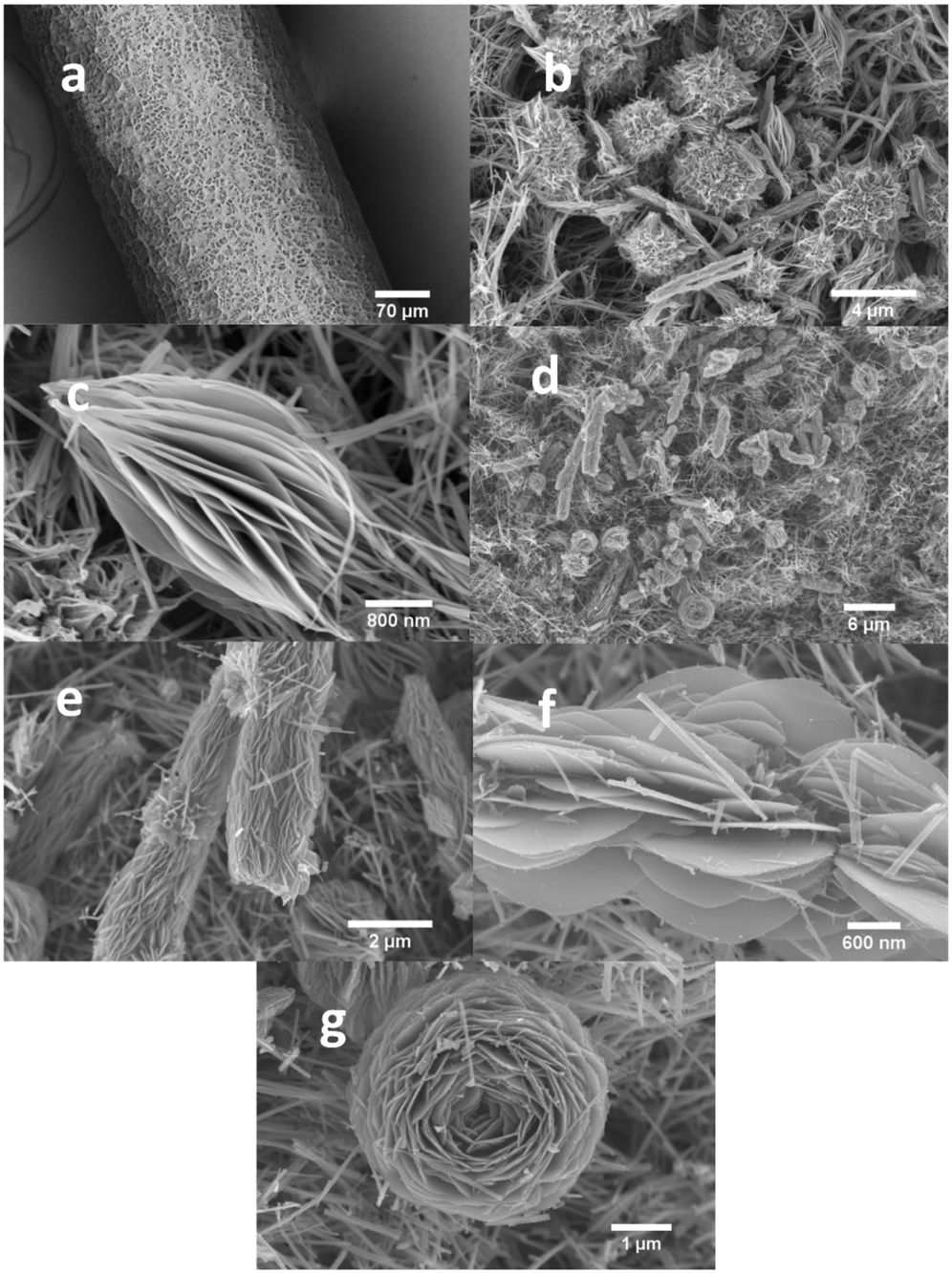

Figure 7**:** SEM Image of Flower and Cactus like TiO2

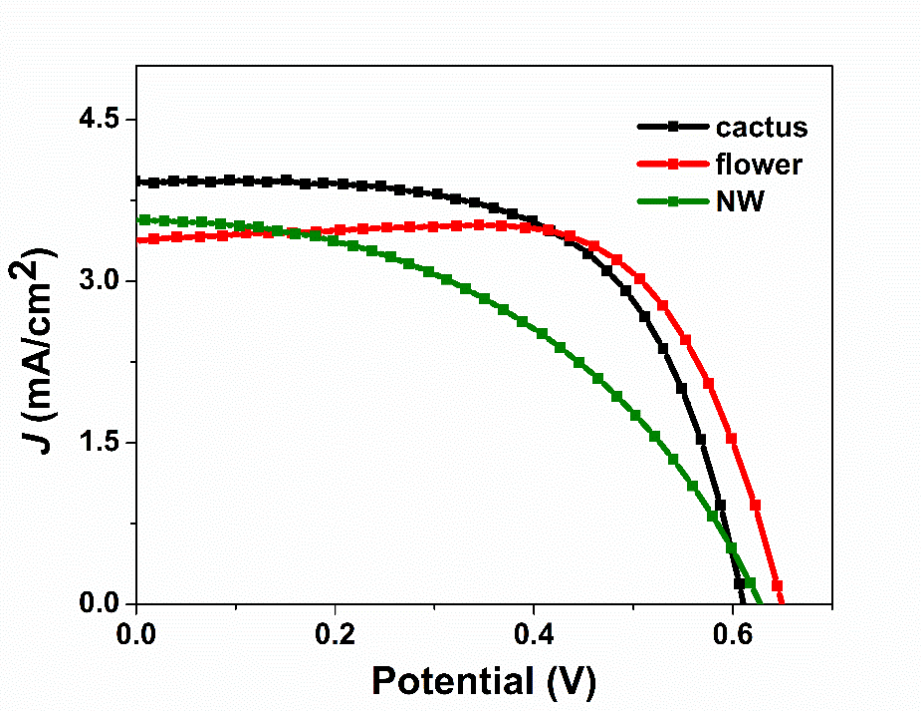

Figure 8: *J-V* Plot of Flower and Cactus like TiO_2

Carbon Fiber Coated with Ni-Co-Se Alloy as the Counter Electrode

Preparation of photoanode

For photoanode preparation several Ti wires (φ = 250 μm) were cleaned by ultrasonicating in ethanol, acetone, and propanol for 15 minutes subsequently. After that, a NaOH solution of 2.5 M has been prepared. 30 mL of this NaOH solution has been put into a Teflon-lined stainless-steel autoclave and the cleaned Ti wires have been immersed into them. The reactor was subsequently placed into a furnace at 220°C for 15-24 hours. After that the reactor was cooled down to room temperature and the wires were washed thoroughly with acetone. Then the wires were put into a 1M HCl solution for 1 hour. The wires were then again washed thoroughly with acetone to get Ti wire with TiO_2 nanowires (NWs). These Ti wires with

TiO_2 NWs were used as the photoanode. For the counter electrode (CE) commercial carbon fiber tow has been used as the substrate.

Preparation of Co-Ni-Se Hollow Microspheres

0.757g of $Co(NO_3)_26H_2O$ [Cobalt(II) Nitrate Hexahydrate], 0.378g of $Ni(NO_3)_26H_2O$ [Nickel(II) Nitrate Hexahydrate] (Ni:Co = 1:2), and 2.6mL of Ethylenediamine was dissolved in 40 mL of distilled water. 0.692g of Na_2SeO_3 [Sodium Selenite] (Ni:Co:Se = 1:2:4) was added to this solution. After an ultrasonic oscillation for 20 mins, the mixed solution was put in a Teflon-lined stainless-steel autoclave reactor. The reactor was put in an electric oven at different temperatures (i.e. 140°C, 160°C, 180°C, 200°) for 24 hours. After that, the reactor was cooled down to room temperature and the precipitate was centrifuged. The precipitate was washed thoroughly with absolute ethanol several times. The precipitate was then dried in an electrical oven at 80°C for 12 hours. The dried products were labeled as Ni-Co-Se-140, Ni-Co-Se-160, Ni-Co-Se-180, and Ni-Co-Se-200.

Preparation of Counter Electrode

Before using the carbon fiber (CF), they have been gone through several treatment to increase their conductivity. First the CF was soaked into acetone for 3 hours to remove any polymer coating present on the surface. Then the CF was washed with milli-Q water, acetone, ethanol respectively under light sonication. Then the CF was kept into a tuber furnace at 300°C for 2 hours under light air flow to thermally degrade the polymer coating. Then the fiber was again washed with milli-Q water, acetone, ethanol respectively under light sonication. The fiber was subsequently kept into a 70% HNO_3 solution under mild stirring for 12 hours. The fiber was again washed with milli-Q water, acetone, ethanol respectively under light sonication. After

drying, the CF was cut into pieces of length 6-7 cm. 5 mg of the Ni-Co-Se sample was dispersed into 2-5 mL of water. The mixed solution was ultrasonically treated to make a uniform dispersion. The CF were then dip coated using this solution and labeled as CF-140, CF-160, CF-180, -CF-200.

Fabrication of FDSSC

The photoanodes prepared on Ti wire were soaked into 0.5 mM N719 dye solution (solvent mixture of acetonitrile and tert-butyl alcohol in a volume ratio of 1:1) for 24 hours. After that, the photoanodes were washed with acetonitrile to remove excess dye. The different CEs were wrapped around the photoanodes. The assembly was inserted into a glass capillary and an electrolyte was injected into the capillary. The electrolyte was prepared by dissolving 0.5 M LiI, 0.05 M I_2, and 0.5 M tert-butyl pyridine and brought up to 10 ml volume in 3-methoxy propionitrile. 5 wt% poly (vinylidene fluoride-co-hexafluoropropylene) was added to this solution. The mixed solution was dissolved overnight with mild heating and vigorous stirring to make a homogeneous solution.

Morphological and Photovoltaic Characterizations: The morphological characterization has been done using scanning electron microscopy (EVO LS10 STEM). X-ray diffraction (XRD) measurements were conducted using a "BRUKER™ D8 X-ray Diffractometer" with a Cu Kα1 radiation (λ = 0.15406 nm, 40 kV, 40 mA). The scanning mode was set to 2θ, and the scanning range was from 10° to 90° with a scanning step size of 0.04° and scanning rate of 1.0° min^{-1}. The photocurrent-voltage measurements were carried out using a VersaSTAT3 potentiostat (Princeton Applied Research) running cyclic voltammetry with a scan rate of 50 $mV{\cdot}s^{-1}$. A Honle

solar simulator 400, with an AM 1.5G spectrum (100 mW/cm^2) was used to simulate sunlight for irradiating the cells.

Result and Discussion

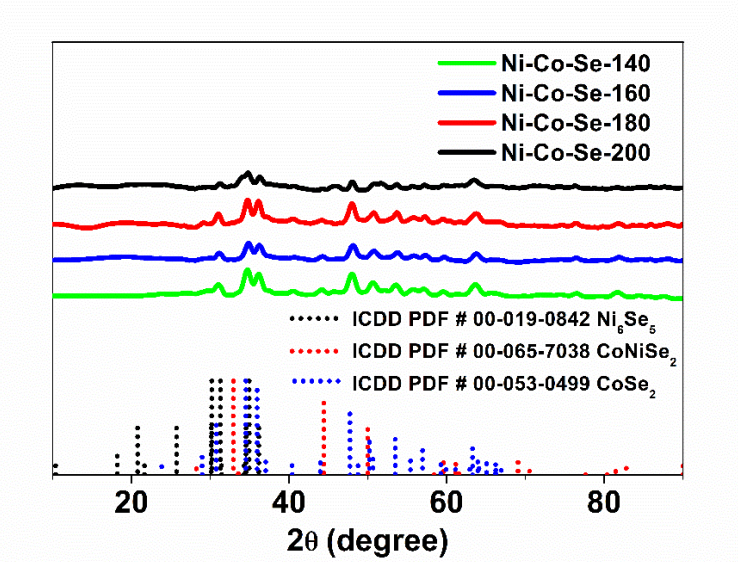

Figure 9: XRD patterns of the samples Ni-Co-Se-140, Ni-Co-Se-160, Ni-Co-Se-180, Ni-Co-Se-200.

Figure 9 shows the XRD patterns of the Ni-Co-Se alloys synthesized at different hydrothermal reaction temperature. It is evident that all the samples show very similar peaks to each other. The different peaks can be successfully assigned to the orthorhombic $CoSe_2$ (JCPDS PDF no. 10-408) and a small fraction can be assigned to orthorhombic Ni_6Se_5 (JCPDS PDF no. 19-842). Apart from these peaks no other peaks are present in the pattern as shown in SI (Supporting Information). The well-defined peaks that appear at 30.1°, 34.5°, 35.2°, 48.0°, 50.1°, 54.5°, and 63.5° corresponds to orthorhombic $CoSe_2$ (110), (111), (012), (121), (211), (220), and

(043) crystal planes respectively. These values agree with the previous report[33]. The peaks at 30.0°, 31.0°, 35.1°, 36.9° corresponds to orthorhombic Ni_6Se_5 (004), (040), (025), (113). In case of Ni-Co-Se-160 another set of peaks are found in the pattern which can be successfully assigned to the hexagonal CoNiSe2 (JCPDS PDF no. 65-7038). The peaks at 34.2°, 44.4°, 50.0°, 62.0° corresponds to (101), (102), (110), (202) planes. So, the XRD patterns of the synthesized alloy should contain only the orthorhombic crystal structure except for the Ni-Co-Se-160 which should contain additional hexagonal crystal structure. It looks like the temperature does not have a significant affect on the crystal structure. However, in case of Ni-Co-Se-200 the peaks intensity seems like to reduce slightly, which implies that increased temperature reduces crystallinity.

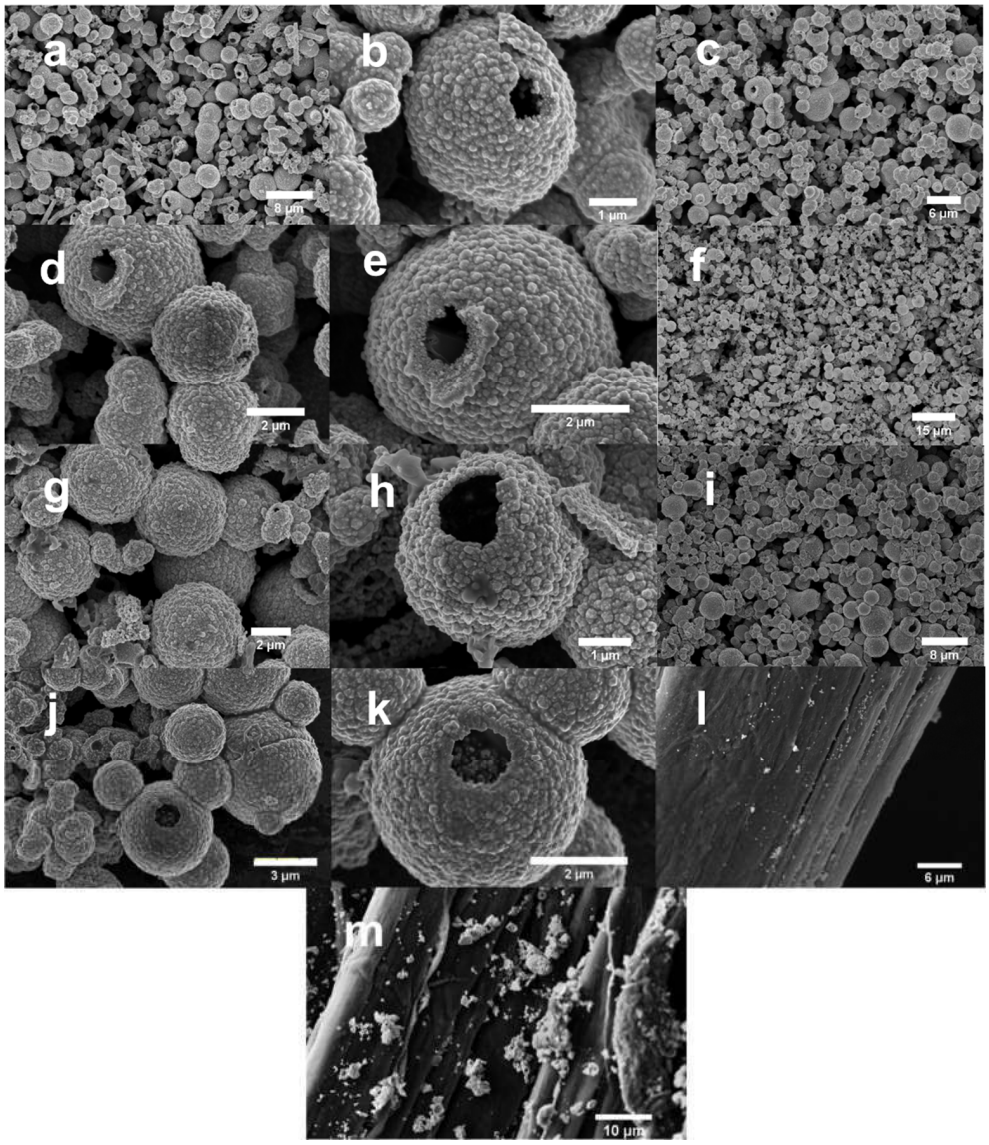

Figure 10: SEM images of Ni-Co-Se synthesized at different hydrothermal reaction temperature, (a,b) Ni-Co-Se-140, (c-e) Ni-Co-Se-160, (f-h) Ni-Co-Se-180, (i-k) Ni-Co-Se-200, (l) CF, (m) CF coated with Ni-Co-Se alloy.

The structural morphologies of the alloys have been done by taking SEM image of the samples prepared at different hydrothermal reaction temperatures. Figure 10 (a, c, f, i) shows the

SEM images of the synthesized allows in bulk. Figure 10 (a) reveal that apart from the spherical allows there are still a significant number of stick-like hollow alloy structures. However, the formation of spherical alloys increases with increasing temperature. While looking at individual microspheres they seem to be not affected much by the different hydrothermal reaction temperatures. The surface of the microspheres seems to rough due to the crosslinked nanoparticles and no smooth surface is visible in the SEM images. The microspheres again connect with each other forming a network. Some irregular structures are also visible which implies the formation of microspheres was incomplete in those locations. The stability of the microspheres at different hydrothermal reaction temperature is very much evident, as no broken or honeycomblike structures are present. Figure 10 (l) shows a portion of bare CF which slightly rough, which is required for the deposition of the Ni-Co-Se allows. The CF were filament initially. While making counter electrode they have been twisted to make then thin fiber like structure. The roughness appears due to the twisting of the filament. Figure 10 (m) shows the successful anchoring of the alloys on the CF.

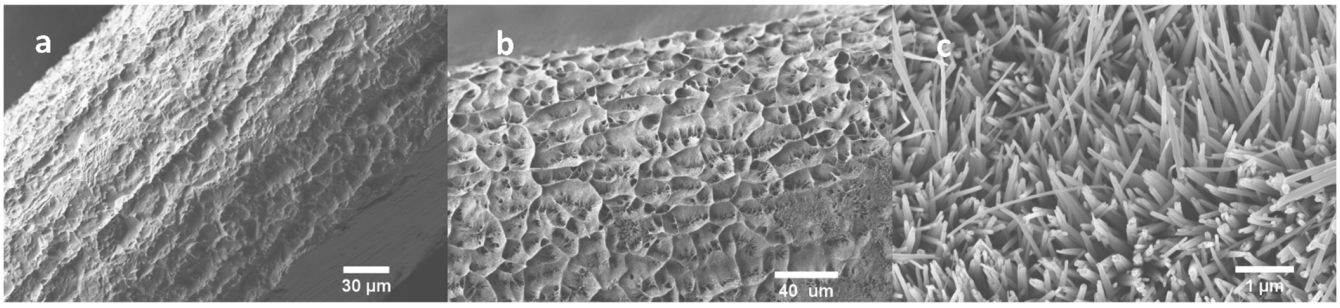

Figure 11: (a) Bare Ti wire, (b) Ti wire coated with TiO_2 NW, (c) zoomed view of individual NW

Figure 11 shows the SEM image of photoanode. Figure a shows bare surface of Ti wire before the NW growth. The Ti wire reacts with NaOH to form $Na_2Ti_2O_53H_2O$ which after the HCl treatment converts to $TiO_2(H_2O)_5$. The annealing treatment removes the water molecules to eventually yield TiO_2 NW[34]. From Figure b and c, it can be seen that the Ti thread is uniformly covered with TiO_2 NW and grown vertically as the aligned structure.

The Formation Mechanism for the Ni-Co-Se Hollow Microspheres

Based on the above observations and studying the previous literature the formation mechanism of Ni-Co-Se hollow microspheres can be proposed in the following way. Ethylenediamine (EDA) plays a significant role in the formation of final desired product. As EDA possess functional groups -NH_2 at both ends, it acts as a powerful chelating agent. It forms a stable chelating mixture by forming bonds with Ni^{2+} and Co^{2+} ions as is also evident from the change of color of the reaction mixture from pale red to dark brown[35]. EDA also pays an important role in determining the surface morphology of the final product by controlling

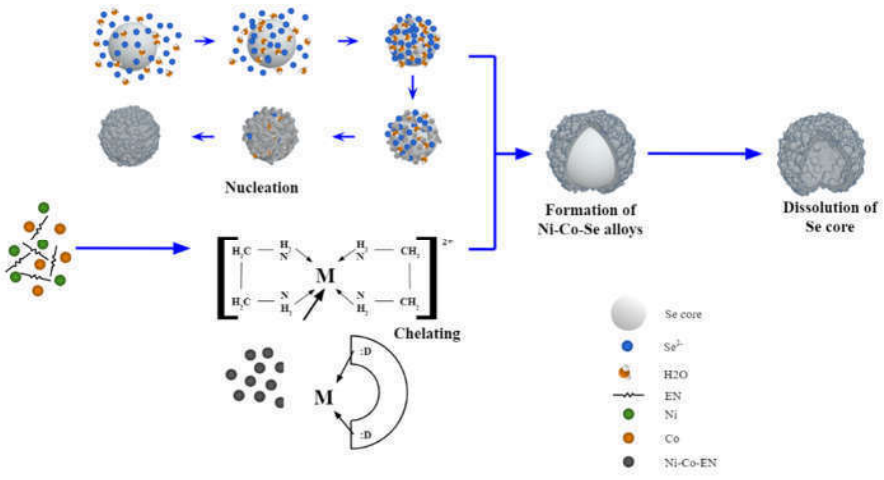

Figure 12: Formation mechanism of Ni-Co-Se hollow microspheres.

the hollow microsphere growth[36-37]. After forming the chelating complex, it can control the release rate of Ni and Co ions from the complex and thus improves the hollow microsphere morphology by lowering the Ni-Co-Se powder generation. Sodium selenite acts as the Se source in this reaction and gets reduced by Co^{2+} or EDA to form Se core, which is also evident during the experiment as the gray Se powder is produced immediately upon adding sodium selenite in the solution[37]. The bimetallic chelates containing the Ni and Co ion gets attached with Se core. Further reaction occurs through the mutual diffusion of the Se core and the chelating complex to form Ni-Co-Se particles. Subsequently a bridged structure is formed and through around the Se core with reaction temperature increasing. As a result of this process, the Se core disappears and the hollow Ni-Co-Se microspheres are formed. This in situ nucleation involves a growth driven force for the formation of the hollow microspheres[38-41]. During the process, the Se^{2-} in the solution also bonds with the atoms on the growing Se core by van der Waals. However, this force is weak compared to the electrostatic attraction between the polar water molecule and Se^{2-} ions. As a result, once the Se^{2-} ions bond to the Se core they are pulled back instantly to the solution. Hence, the surface of the product Ni-Co-Se hollow microspheres appear rough.

Photovoltaic Characterization

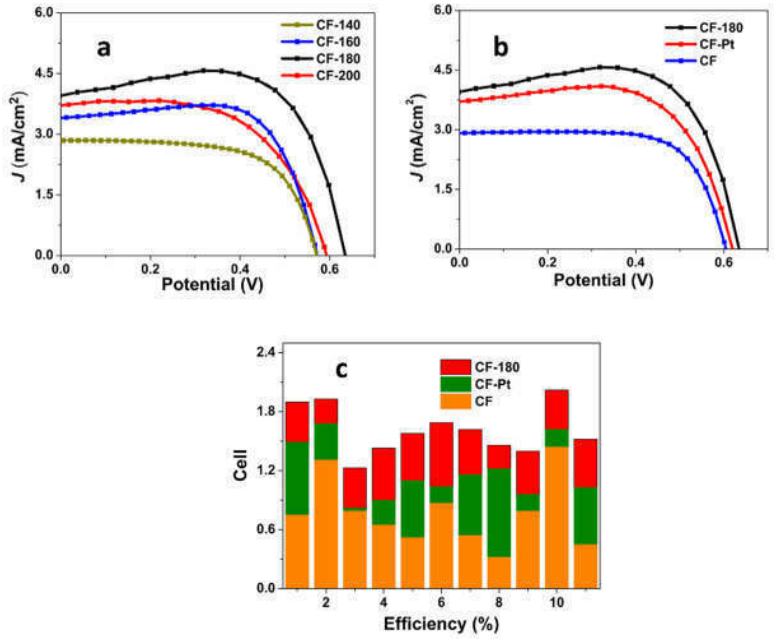

Figure 13: a) comparison of *J-V* plot between CF-140, CF-160, CF-180, and CF-200, b) comparison of *J-V* plot between CF-180, CF-Pt, and CF, c) a performance analysis of CF-180, CF-Pt, and CF based on 11 cells using each of the CE.

Figure 13-a, b represents the photovoltaic performance of the counter electrodes coated with different types of hollow microsphere alloys. As the hydrothermal temperature increases both the J_{sc} and V_{oc} keeps increasing and the after 180°C, the performance again drops. The reason can be attributed to the fact that, with increased hydrothermal reaction time, the hollow microsphere growth is achieved perfectly, and the crystallinity also increases. At lower hydrothermal reaction, the hollow sphere growth is incomplete leading to a lot of hollow sticklike structures. The best performance of the CE has been found for a hydrothermal reaction of 180°C. Apart from the successful formation of the hollo spheres the other reason can be

attributed to the efficient reduction of the I_3^- to I^-. the reduced charge transfer resistance at the electrolyte and CE surface is another reason for the improved performance.

Table 3: Photovoltaic properties of FDSSC using different CEs.

CE	J_{sc}, mA/cm^2	V_{oc}, Volt	Efficiency, %	FF
CF-140	2.83	0.57	1.08	0.67
CF-160	3.76	0.59	1.41	0.62
CF-180	3.96	0.63	2.03	0.53
CF-200	3.39	0.57	1.51	0.8
CF-Pt	3.68	0.62	1.69	0.74
CF	2.88	0.6	1.27	0.73

To test the flexibility of the devices, performance of the cells after bending 10 times and after illuminating for multiple radiation cycles has been perfromed. In both the cases, the devices significant retain their performance. The reason can be attributed to the increased soomthness and fiber like nature of the CF and its exellent stability against corrision by I_3^-/I^- electrolyte.

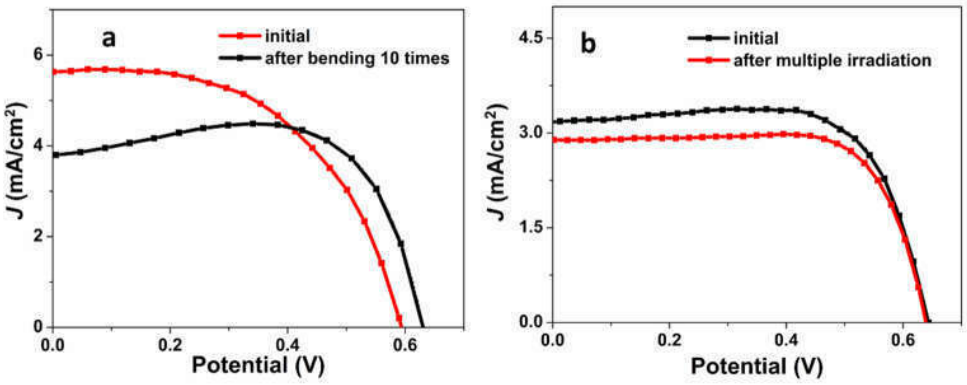

Figure 14: a) comparison of performance after bending 10 times c) comparison of performance after irradiating the cell for 10 times

CHAPTER IV

SUMMARY AND CONCLUSIONS

In conclusion, fabrication of a novel hierarchical photoanode with TiO_2 nano-tree array and plasmonic Ag NPs has been reported. A two-step facile hydrothermal route has been assigned to obtain the desired TiO_2 morphology and a photon-assisted and solution processed synthesis route has been used to deposit the Ag nanoparticles. The device using the resultant photoanode gave a 16.1% increase in efficiency compared to bare NTA based device and 81.6% increase in efficiency compared to the corresponding NWA based device. A relative comparison study of the performance attained form three types of photoanode based device has been performed. Optimization of different parameters have also been done. The higher internal surface area, improved dye loading and light scattering, SPR effect of Ag-NPs has been identified as the reasons behind the higher performance of the novel photoanode among many other reasons. To test the applicability of the device bending test, comparison with length and in ice has also been performed. Despite a slight drop in the performance, all three tests point out towards a variety of application where the photoanodes can be suitable. Further study in this area can be done to better understand the experimental and operational variables. For example, a study could be conducted to find out the optimum concentration of $AgNO_3$ solution for depositing Ag-NPs.

A thorough investigation on the morphological characterization of the nano-tree arrays and size dependent gradient distribution of the Ag-NPs could also be done.

REFERENCES

[1] M. Hatamvand, E. Kamrani, M. Lira-Cantú, M. Madsen, B.R. Patil, P. Vivo, M.S. Mehmood, A. Numan, I. Ahmed, Y. Zhan, Recent advances in fiber-shaped and planar-shaped textile solar cells, Nano Energy 71 (2020) 104609.

[2] M. Freitag, J. Teuscher, Y. Saygili, X. Zhang, F. Giordano, P. Liska, J. Hua, S.M. Zakeeruddin, J.-E. Moser, M. Grätzel, Dye-sensitized solar cells for efficient power generation under ambient lighting, Nature Photonics 11 (2017) 372.

[3] J. Zhang, Z. Wang, X. Li, J. Yang, C. Song, Y. Li, J. Cheng, Q. Guan, B. Wang, Flexible Platinum-Free Fiber-Shaped Dye Sensitized Solar Cell with 10.28% Efficiency, ACS Applied Energy Materials 2 (2019) 2870-2877.

[4] K. Zhu, N.R. Neale, A. Miedaner, A.J. Frank, Enhanced charge-collection efficiencies and light scattering in dye-sensitized solar cells using oriented TiO2 nanotubes arrays, Nano Lett. 7 (2007) 69-74.

[5] S.H. Kang, S.H. Choi, M.S. Kang, J.Y. Kim, H.S. Kim, T. Hyeon, Y.E. Sung, Nanorod-based dye-sensitized solar cells with improved charge collection efficiency, Adv. Mater. 20 (2008) 54-58.

[6] B. Liu, E.S. Aydil, Growth of Oriented Single-Crystalline Rutile TiO2 Nanorods on Transparent Conducting Substrates for Dye-Sensitized Solar Cells, J. Am. Chem. Soc. 131 (2009) 3985-3990.

[7] Q.L. Huang, G. Zhou, L. Fang, L.P. Hu, Z.S. Wang, TiO2 nanorod arrays grown from a mixed acid medium for efficient dye-sensitized solar cells, Energy Environ. Sci. 4 (2011) 2145-2151.

[8] P.P. Sun, X.T. Zhang, X.P. Liu, L.L. Wang, C.H. Wang, J.K. Yang, Y.C. Liu, Growth of single-crystalline rutile TiO2 nanowire array on titanate nanosheet film for dye-sensitized solar cells, J. Mater. Chem. 22 (2012) 6389-6393.

[9] M. Iraj, F.D. Nayeri, E. Asl-Soleimani, K. Narimani, Controlled growth of vertically aligned TiO2 nanorod arrays using the improved hydrothermal method and their application to dye-sensitized solar cells, J. Alloy. Compd. 659 (2016) 44-50.

[10] Z. Wei, Y. Yao, T. Huang, A.S. Yu, Solvothermal growth of well-aligned TiO2 nanowire arrays for dye-sensitized solar cell: dependence of morphology and vertical orientation upon substrate pretreatment, Int. J. Electrochem. Sci. 6 (2011) 1871-1879.

[11] W.W. Liu, H. Lu, M. Zhang, M. Guo, Controllable preparation of TiO2 nanowire arrays on titanium mesh for flexible dye-sensitized solar cells, Appl. Surf. Sci. 347 (2015) 214-223.

[12] M.Q. Lv, D.J. Zheng, M.D. Ye, L. Sun, J. Xiao, W.X. Guo, C.J. Lin, Densely aligned rutile TiO2 nanorod arrays with high surface area for efficient dye-sensitized solar cells, Nanoscale 4 (2012) 5872-5879.

[13] Z. Wei, R.S. Li, T. Huang, A.S. Yu, Fabrication of morphology controllable rutile TiO2 nanowire arrays by solvothermal route for dye-sensitized solar cells, Electrochim. Acta 56 (2011) 7696-7702.

[14] Y.M. Xiao, J.H. Wu, G.T. Yue, J.M. Lin, M.L. Huang, L.Q. Fan, Z. Lan, Preparation of Single-Crystalline TiO2 Nanowires and Their Application in Flexible Dye-Sensitized Solar Cells, Acta Phys.-Chim. Sin. 28 (2012) 578-584.

[15] G.C. Liu, H. Wang, M.X. Wang, W.B. Liu, R.E.A. Ardhi, D.C. Zou, J.K. Lee, Study on a stretchable, fiber-shaped, and TiO2 nanowire array-based dye-sensitized solar cell with electrochemical impedance spectroscopy method, Electrochim. Acta 267 (2018) 34-40.

[16] M. Law, L.E. Greene, J.C. Johnson, R. Saykally, P.D. Yang, Nanowire dye-sensitized solar cells, Nat. Mater. 4 (2005) 455-459.

[17] K. Zhu, T.B. Vinzant, N.R. Neale, A.J. Frank, Removing structural disorder from oriented TiO2 nanotube arrays: Reducing the dimensionality of transport and recombination in dye-sensitized solar cells, Nano Lett. 7 (2007) 3739-3746.

[18] O.K. Varghese, M. Paulose, C.A. Grimes, Long vertically aligned titania nanotubes on transparent conducting oxide for highly efficient solar cells, Nat. Nanotechnol. 4 (2009) 592-597.

[19] X.J. Feng, K. Zhu, A.J. Frank, C.A. Grimes, T.E. Mallouk, Rapid Charge Transport in Dye-Sensitized Solar Cells Made from Vertically Aligned Single-Crystal Rutile TiO2 Nanowires, Angew. Chem.-Int. Edit. 51 (2012) 2727-2730.

[20] F. Shao, J. Sun, L. Gao, S.W. Yang, J.Q. Luo, Forest-like TiO2 hierarchical structures for efficient dye-sensitized solar cells, J. Mater. Chem. 22 (2012) 6824-6830.

[21] X. Sheng, D.Q. He, J. Yang, K. Zhu, X.J. Feng, Oriented Assembled TiO2 Hierarchical Nanowire Arrays with Fast Electron Transport Properties, Nano Lett. 14 (2014) 1848-1852.

[22] H. Yu, J. Pan, Y. Bai, X. Zong, X.Y. Li, L.Z. Wang, Hydrothermal Synthesis of a Crystalline Rutile TiO2 Nanorod Based Network for Efficient Dye-Sensitized Solar Cells, Chem.-Eur. J. 19 (2013) 13569-13574.

[23] J.Y. Liao, B.X. Lei, H.Y. Chen, D.B. Kuang, C.Y. Su, Oriented hierarchical single crystalline anatase TiO2 nanowire arrays on Ti-foil substrate for efficient flexible dye-sensitized solar cells, Energy Environ. Sci. 5 (2012) 5750-5757.

[24] M.R. Subramaniam, S. Devanathan, D. Kumaresan, Synthesis of micrometer-sized hierarchical rutile TiO2 flowers and their application in dye sensitized solar cells, RSC Adv. 4 (2014) 36791-36799.

[25] B.X. Lei, X.F. Zheng, H.K. Qiao, Y. Li, S.N. Wang, G.L. Huang, Z.F. Sun, A novel hierarchical homogeneous nanoarchitecture of TiO2 nanosheets branched TiO2 nanosheet arrays for high efficiency dye-sensitized solar cells, Electrochim. Acta 149 (2014) 264-270.

[26] C. Clavero, Plasmon-induced hot-electron generation at nanoparticle/metal-oxide interfaces for photovoltaic and photocatalytic devices, Nat. Photonics 8 (2014) 95-103.

[27] M.W. Knight, Y.M. Wang, A.S. Urban, A. Sobhani, B.Y. Zheng, P. Nordlander, N.J. Halas, Embedding plasmonic nanostructure diodes enhances hot electron emission, Nano Lett. 13 (2013) 1687-1692.

[28] J. Hofmann, W. Steinman, Plasma resonance in photoemission of silver, Physica Status Solidi 30 (1968) K53-K56.

[29] J.G. Endriz, W.E. Spicer, Surface-plasmon-one-electron decay and its observation in photoemission, Physical Review Letters 24 (1970) 64-68.

[30] J. Lehmann, M. Merschdorf, W. Pfeiffer, A. Thon, S. Voll, G. Gerber, Surface plasmon dynamics in silver nanoparticles studied by femtosecond time-resolved photoemission, Physical Review Letters 85 (2000) 2921-2924.

[31] S. Linic, P. Christopher, D.B. Ingram, Plasmonic-metal nanostructures for efficient conversion of solar to chemical energy, Nat. Mater. 10 (2011) 911-921.

[32] C. Sonnichsen, T. Franzl, T. Wilk, G. von Plessen, J. Feldmann, O. Wilson, P. Mulvaney, Drastic reduction of plasmon damping in gold nanorods, Physical Review Letters 88 (2002) 4.

[33] M. Rycenga, C.M. Cobley, J. Zeng, W.Y. Li, C.H. Moran, Q. Zhang, D. Qin, Y.N. Xia, Controlling the Synthesis and Assembly of Silver Nanostructures for Plasmonic Applications, Chem. Rev. 111 (2011) 3669-3712.

[34] Q.P. Lu, Z.D. Lu, Y.Z. Lu, L.F. Lv, Y. Ning, H.X. Yu, Y.B. Hou, Y.D. Yin, Photocatalytic Synthesis and Photovoltaic Application of Ag-TiO2 Nanorod Composites, Nano Lett. 13 (2013) 5698-5702.

[35] H. Dong, Z.X. Wu, Y.C. Gao, A. El-Shafei, S.Y. Ning, J. Xi, B. Jiao, X. Hou, Silver-loaded anatase nanotubes dispersed plasmonic composite photoanode for dye-sensitized solar cells, Org. Electron. 15 (2014) 2847-2854.

[36] Y.M. Liu, M.L. Zhang, Y. Jiang, Y. Xia, W.W. Sun, X.Z. Zhao, General Strategy to Construct Hierarchical TiO2 Nanorod Arrays coupling with Plasmonic Resonance for Dye-sensitized Solar Cells, Electrochim. Acta 173 (2015) 483-489.

[37] W.J. Yu, W.W. Sun, Y.M. Liu, H.F. Mehnane, H.M. Liu, K. Zhang, B. Cai, W. Liu, S.S. Guo, X.Z. Zhao, Constructed Single-Crystal Rutile TiO2 Cluster and Plasmon Synergistic Effect for Dye-Sensitized Solar Cells, Electrochim. Acta 180 (2015) 705-711.

[38] Y. Wang, Z. Li, Y. Cao, F. Li, W. Zhao, X.Q. Liu, J.B. Yang, Fabrication of novel Ag-TiO2 nanobelts as a photoanode for enhanced photovoltage performance in dye sensitized solar cells, J. Alloy. Compd. 677 (2016) 294-301.

[39] H.H. Hu, J.F. Shen, X.H. Cao, H. Wang, H.R. Lv, Y.C. Zhang, W.Z. Zhu, J.H. Zhao, C. Cui, Photo-assisted deposition of Ag nanoparticles on branched TiO2 nanorod arrays for dye-sensitized solar cells with enhanced efficiency, J. Alloy. Compd. 694 (2017) 653-661.

[40] X. Yu, X. Han, Z.H. Zhao, J. Zhang, W.B. Guo, C.F. Pan, A.X. Li, H. Liu, Z.L. Wang, Hierarchical TiO2 nanowire/graphite fiber photoelectrocatalysis setup powered by a wind-driven nanogenerator: A highly efficient photoelectrocatalytic device entirely based on renewable energy, Nano Energy 11 (2015) 19-27.

[41] L. Chu, L.Y. Li, J. Su, F.F. Tu, N.S. Liu, Y.H. Gao, A general method for preparing anatase TiO2 treelike-nanoarrays on various metal wires for fiber dye-sensitized solar cells, Sci Rep 4 (2014) 6.

[42] L. Chen, Y. Zhou, H. Dai, Z. Li, T. Yu, J. Liu, Z. Zou, Fiber dye-sensitized solar cells consisting of TiO2 nanowires arrays on Ti thread as photoanodes through a low-cost, scalable route, Journal of Materials Chemistry A 1 (2013) 11790-11794.

[43] G. Liu, H. Wang, M. Wang, W. Liu, R.E.A. Ardhi, D. Zou, J.K. Lee, Study on a stretchable, fiber-shaped, and TiO2 nanowire array-based dye-sensitized solar cell with electrochemical impedance spectroscopy method, Electrochimica Acta 267 (2018) 34-40.

[44] F. Shao, J. Sun, L. Gao, S. Yang, J. Luo, Forest-like TiO2 hierarchical structures for efficient dye-sensitized solar cells, J. Mater. Chem. 22 (2012) 6824-6830.

[45] F. Shao, J. Sun, L. Gao, S. Yang, J. Luo, Growth of Various TiO2 Nanostructures for Dye-Sensitized Solar Cells, The Journal of Physical Chemistry C 115 (2011) 1819-1823.

[46] E. Galoppini, J. Rochford, H. Chen, G. Saraf, Y. Lu, A. Hagfeldt, G. Boschloo, Fast electron transport in metal organic vapor deposition grown dye-sensitized ZnO nanorod solar cells, The Journal of Physical Chemistry B 110 (2006) 16159-16161.

[47] A.B. Martinson, M.S. Góes, F. Fabregat-Santiago, J. Bisquert, M.J. Pellin, J.T. Hupp, Electron transport in dye-sensitized solar cells based on ZnO nanotubes: evidence for highly efficient charge collection and exceptionally rapid dynamics, The Journal of Physical Chemistry A 113 (2009) 4015-4021.

[48] B.H. Lee, M.Y. Song, S.-Y. Jang, S.M. Jo, S.-Y. Kwak, D.Y. Kim, Charge transport characteristics of high efficiency dye-sensitized solar cells based on electrospun TiO2 nanorod photoelectrodes, The Journal of Physical Chemistry C 113 (2009) 21453-21457.

[49] X. Feng, K. Shankar, O.K. Varghese, M. Paulose, T.J. Latempa, C.A. Grimes, Vertically aligned single crystal TiO2 nanowire arrays grown directly on transparent conducting oxide coated glass: synthesis details and applications, Nano letters 8 (2008) 3781-3786.

[50] Z.J. Zhou, J.Q. Fan, X. Wang, W.H. Zhou, Z.L. Du, S.X. Wu, Effect of highly ordered single-crystalline TiO2 nanowire length on the photovoltaic performance of dye-sensitized solar cells, ACS applied materials & interfaces 3 (2011) 4349-4353.

[51] S. Ito, S.M. Zakeeruddin, R. Humphry-Baker, P. Liska, R. Charvet, P. Comte, M.K. Nazeeruddin, P. Péchy, M. Takata, H. Miura, High-efficiency organic-dye-sensitized solar cells controlled by nanocrystalline-TiO2 electrode thickness, Advanced Materials 18 (2006) 1202-1205.

[52] M. Kao, H. Chen, S. Young, C. Kung, C. Lin, The effects of the thickness of TiO2 films on the performance of dye-sensitized solar cells, Thin Solid Films 517 (2009) 5096-5099.

[53] D.K. Roh, W.S. Chi, H. Jeon, S.J. Kim, J.H. Kim, High efficiency solid-state dye-sensitized solar cells assembled with hierarchical anatase pine tree-like TiO2 nanotubes, Advanced Functional Materials 24 (2014) 379-386.

[54] H. Hu, J. Shen, X. Cao, H. Wang, H. Lv, Y. Zhang, W. Zhu, J. Zhao, C. Cui, Photo-assisted deposition of Ag nanoparticles on branched TiO2 nanorod arrays for dye-sensitized solar cells with enhanced efficiency, Journal of Alloys and Compounds 694 (2017) 653-661.

[55] J.M. Herrmann, J. Disdier, P. Pichat, Photoassisted platinum deposition on TiO2 powder using various platinum complexes, The Journal of Physical Chemistry 90 (1986) 6028-6034.

[56] H. Dong, Z. Wu, Y. Gao, A. El-Shafei, S. Ning, J. Xi, B. Jiao, X. Hou, Silver-loaded anatase nanotubes dispersed plasmonic composite photoanode for dye-sensitized solar cells, Organic Electronics 15 (2014) 2847-2854.

[57] X.L. He, G.J. Yang, C.J. Li, M. Liu, S.Q. Fan, Failure mechanism for flexible dye-sensitized solar cells under repeated outward bending: Cracking and spalling off of nano-porous titanium dioxide film, Journal of Power Sources 280 (2015) 182-189.

[58] X. Chen, S.S. Mao, Titanium dioxide nanomaterials: Synthesis, properties, modifications, and applications, Chem. Rev. 107 (2007) 2891-2959.

[59] X.D. Wang, Z.D. Li, J. Shi, Y.H. Yu, One-Dimensional Titanium Dioxide Nanomaterials: Nanowires, Nanorods, and Nanobelts, Chem. Rev. 114 (2014) 9346-9384.

[60] A. Salvador, M.C. Pascual-Marti, J.R. Adell, A. Requeni, J.G. March, Analytical methodologies for atomic spectrometric determination of metallic oxides in UV sunscreen creams, J. Pharm. Biomed. Anal. 22 (2000) 301-306.

[61] R. Zallen, M.P. Moret, The optical absorption edge of brookite TiO2, Solid State Commun. 137 (2006) 154-157.

[62] J.H. Braun, A. Baidins, R.E. Marganski, TiO2 pigment technology - a review, Prog. Org. Coat. 20 (1992) 105-138.

[63] S.A. Yuan, W.H. Chen, S.S. Hu, Fabrication of TiO2 nanoparticles/surfactant polymer complex film on glassy carbon electrode and its application to sensing trace dopamine, Mater. Sci. Eng. C-Biomimetic Supramol. Syst. 25 (2005) 479-485.

[64] J.T. Jiu, S. Isoda, F.M. Wang, M. Adachi, Dye-sensitized solar cells based on a single-crystalline TiO2 nanorod film, J. Phys. Chem. B 110 (2006) 2087-2092.

[65] B. Liu, E.S. Aydil, Growth of Oriented Single-Crystalline Rutile TiO2 Nanorods on Transparent Conducting Substrates for Dye-Sensitized Solar Cells, J. Am. Chem. Soc. 131 (2009) 3985-3990.

[66] U. Bach, D. Lupo, P. Comte, J.E. Moser, F. Weissortel, J. Salbeck, H. Spreitzer, M. Gratzel, Solid-state dye-sensitized mesoporous TiO2 solar cells with high photon-to-electron conversion efficiencies, Nature 395 (1998) 583-585.

[67] M. Law, L.E. Greene, A. Radenovic, T. Kuykendall, J. Liphardt, P.D. Yang, ZnO-Al2O3 and ZnO-TiO2 core-shell nanowire dye-sensitized solar cells, J. Phys. Chem. B 110 (2006) 22652-22663.

[68] L.E. Greene, M. Law, B.D. Yuhas, P.D. Yang, ZnO-TiO2 core-shell nanorod/P3HT solar cells, Journal of Physical Chemistry C 111 (2007) 18451-18456.

[69] J.W. Liu, Y.T. Kuo, K.J. Klabunde, C. Rochford, J. Wu, J. Li, Novel Dye-Sensitized Solar Cell Architecture Using TiO2-Coated Vertically Aligned Carbon Nanofiber Arrays, ACS Appl. Mater. Interfaces 1 (2009) 1645-1649.

[70] J. Burschka, N. Pellet, S.J. Moon, R. Humphry-Baker, P. Gao, M.K. Nazeeruddin, M. Gratzel, Sequential deposition as a route to high-performance perovskite-sensitized solar cells, Nature 499 (2013) 316-319.

[71] A.H. Ip, S.M. Thon, S. Hoogland, O. Voznyy, D. Zhitomirsky, R. Debnath, L. Levina, L.R. Rollny, G.H. Carey, A. Fischer, K.W. Kemp, I.J. Kramer, Z.J. Ning, A.J. Labelle, K.W. Chou, A. Amassian, E.H. Sargent, Hybrid passivated colloidal quantum dot solids, Nat. Nanotechnol. 7 (2012) 577-582.

[72] S. Gunes, H. Neugebauer, N.S. Sariciftci, Conjugated polymer-based organic solar cells, Chem. Rev. 107 (2007) 1324-1338.

[73] J.Y. Kim, S.H. Kim, H.H. Lee, K. Lee, W.L. Ma, X. Gong, A.J. Heeger, New architecture for high-efficiency polymer photovoltaic cells using solution-based titanium oxide as an optical spacer, Adv. Mater. 18 (2006) 572-576.

[74] E. Roduner, Size matters: why nanomaterials are different, Chem. Soc. Rev. 35 (2006) 583-592.

[75] T. Lopez-Luke, A. Wolcott, L.P. Xu, S.W. Chen, Z.H. Wcn, J.H. Li, E. De La Rosa, J.Z. Zhang, Nitrogen-doped and CdSe quantum-dot-sensitized nanocrystalline TiO2 films for solar energy conversion applications, Journal of Physical Chemistry C 112 (2008) 1282-1292.

[76] M. Law, L.E. Greene, J.C. Johnson, R. Saykally, P.D. Yang, Nanowire dye-sensitized solar cells, Nat. Mater. 4 (2005) 455-459.

[77] K. Zhu, N.R. Neale, A. Miedaner, A.J. Frank, Enhanced charge-collection efficiencies and light scattering in dye-sensitized solar cells using oriented TiO2 nanotubes arrays, Nano Lett. 7 (2007) 69-74.

[78] D. Chen, H. Zhang, S. Hu, J.H. Li, Preparation and enhanced photoelectrochemical performance of coupled bicomponent ZnO-TiO2 nanocomposites, Journal of Physical Chemistry C 112 (2008) 117-122.

[79] S.H. Kang, S.H. Choi, M.S. Kang, J.Y. Kim, H.S. Kim, T. Hyeon, Y.E. Sung, Nanorod-based dye-sensitized solar cells with improved charge collection efficiency, Adv. Mater. 20 (2008) 54-58.

[80] W.G. Yang, F.R. Wan, Y.L. Wang, C.H. Jiang, Achievement of 6.03% conversion efficiency of dye-sensitized solar cells with single-crystalline rutile TiO2 nanorod photoanode, Appl. Phys. Lett. 95 (2009) 133121.

[81] K. Fujihara, A. Kumar, R. Jose, S. Ramakrishna, S. Uchida, Spray deposition of electrospun TiO2 nanorods for dye-sensitized solar cell, Nanotechnology 18 (2007) 365709.

[82] F. Shao, J. Sun, L.A. Gao, S.W. Yang, J.Q. Luo, Growth of Various TiO2 Nanostructures for Dye-Sensitized Solar Cells, Journal of Physical Chemistry C 115 (2011) 1819-1823.

[83] R. Wang, X. Cai, F.L. Shen, Preparation of TiO2 hollow microspheres by a novel vesicle template method and their enhanced photocatalytic properties, Ceram. Int. 39 (2013) 9465-9470.

[84] F.B. Li, X.Z. Li, M.F. Hou, K.W. Cheah, W.C.H. Choy, Enhanced photocatalytic activity of Ce3+-TiO2 for 2-mercaptobenzothiazole degradation in aqueous suspension for odour control, Appl. Catal. A-Gen. 285 (2005) 181-189.

[85] J.G. Yu, J.C. Yu, W.K. Ho, M.K.P. Leung, B. Cheng, G.K. Zhang, X.J. Zhao, Effects of alcohol content and calcination temperature on the textural properties of bimodally mesoporous titania, Appl. Catal. A-Gen. 255 (2003) 309-320.

[86] J. Yun, D. Jin, Y.S. Lee, H.I. Kim, Photocatalytic treatment of acidic waste water by electrospun composite nanofibers of pH-sensitive hydrogel and TiO2, Mater. Lett. 64 (2010) 2431-2434.

[87] C.K. Chan, H.L. Peng, G. Liu, K. McIlwrath, X.F. Zhang, R.A. Huggins, Y. Cui, High-performance lithium battery anodes using silicon nanowires, Nat. Nanotechnol. 3 (2008) 31-35.

[88] S.W. Boettcher, J.M. Spurgeon, M.C. Putnam, E.L. Warren, D.B. Turner-Evans, M.D. Kelzenberg, J.R. Maiolo, H.A. Atwater, N.S. Lewis, Energy-Conversion Properties of Vapor-Liquid-Solid-Grown Silicon Wire-Array Photocathodes, Science 327 (2010) 185-187.

[89] Y.Z. Wang, X. Hong, G.Z. Wang, X.P. Wang, Fabrication and photocatalysis of TiO2 flower-like nanostructures, Chin. J. Chem. Phys. 19 (2006) 559-562.

[90] R.S. Hyam, R.K. Bhosale, W. Lee, S.H. Han, B. Hannoyer, S.B. Ogale, Room Temperature Synthesis of Rutile TiO2 Hierarchical Nanoneedle Flower Morphology for Dye Sensitized Solar Cell, J. Nanosci. Nanotechnol. 10 (2010) 5894-5898.

[91] Q.J. Xiang, J.G. Yu, Photocatalytic Activity of Hierarchical Flower-Like TiO2 Superstructures with Dominant {001} Facets, Chin. J. Catal. 32 (2011) 525-531.

[92] N.X. Xu, L. Hu, Q.L. Zhang, X.R. Xiao, H. Yang, E.J. Yu, Significantly Enhanced Dielectric Performance of Poly(vinylidene fluoride-co-hexafluoropylene)-based Composites Filled with Hierarchical Flower-like TiO2 Particles, ACS Appl. Mater. Interfaces 7 (2015) 27373-27381.

[93] L. Zhao, C. Zhong, Y.L. Wang, S.M. Wang, B.H. Dong, L. Wan, Ag nanoparticle-decorated 3D flower-like TiO2 hierarchical microstructures composed of ultrathin nanosheets

and enhanced photoelectrical conversion properties in dye-sensitized solar cells, J. Power Sources 292 (2015) 49-57.

[94] H.L. Li, T.D. Li, H.X. Liu, B.B. Huang, Q. Zhang, Hierarchical flower-like nanostructures of anatase TiO2 nanosheets dominated by {001} facets, J. Alloy. Compd. 657 (2016) 1-7.

[95] Y.P. Que, J. Weng, L.H. Hu, J.H. Wu, S.Y. Dai, High open voltage and superior light-harvesting dye-sensitized solar cells fabricated by flower-like hierarchical TiO2 composed with highly crystalline nanosheets, J. Power Sources 307 (2016) 138-145.

[96] L.Y. Zong, G.D. Zhang, J.H. Zhao, F. Dong, J.Y. Zhang, Z.C. Tang, Morphology-controlled synthesis of 3D flower-like TiO2 and the superior performance for selective catalytic reduction of NOx with NH3, Chem. Eng. J. 343 (2018) 500-511.

[97] H.X. Liu, L.N. Zhang, T.D. Li, A Study of Controllable Synthesis and Formation Mechanism on Flower-Like TiO2 with Spherical Structure, Crystals 8 (2018) 466.

[98] J.X. Zhang, Z.P. Wang, X.L. Li, J. Yang, C.H. Song, Y.P. Li, J.L. Cheng, Q. Guan, B. Wang, Flexible Platinum-Free Fiber-Shaped Dye Sensitized Solar Cell with 10.28% Efficiency, ACS Appl. Energ. Mater. 2 (2019) 2870-2877.

[99] G.C. Liu, H. Wang, M.X. Wang, W.B. Liu, R.E.A. Ardhi, D.C. Zou, J.K. Lee, Study on a stretchable, fiber-shaped, and TiO2 nanowire array-based dye-sensitized solar cell with electrochemical impedance spectroscopy method, Electrochim. Acta 267 (2018) 34-40.

[100] L. Chu, L.Y. Li, J. Su, F.F. Tu, N.S. Liu, Y.H. Gao, A General Method for Preparing Anatase TiO2 Treelike-Nanoarrays on Various Metal Wires for Fiber Dye-Sensitized Solar Cells, Sci Rep 4 (2014) 4420.

[101] Hatamvand, M.; Kamrani, E.; Lira-Cantu, M.; Madsen, M.; Patil, B. R.; Vivo, P.; Mehmood, M. S.; Numan, A.; Ahmed, I.; Zhan, Y. Q., Recent advances in fiber-shaped and planar-shaped textile solar cells. Nano Energy 2020, 71, 17.

[102] Gerische.H; Michelbe.Me; Rebentro.F; Tributsc.H, SENSITIZATION OF CHARGE INJECTION INTO SEMICONDUCTORS WITH LARGE BAND GAP. Electrochim. Acta 1968, 13 (6), 1509-&.

[103] Oregan, B.; Gratzel, M., A LOW-COST, HIGH-EFFICIENCY SOLAR-CELL BASED ON DYE-SENSITIZED COLLOIDAL TIO2 FILMS. Nature 1991, 353 (6346), 737-740.

[104] Gratzel, M., Photoelectrochemical cells. Nature 2001, 414 (6861), 338-344.

[105]. Yella, A.; Lee, H. W.; Tsao, H. N.; Yi, C. Y.; Chandiran, A. K.; Nazeeruddin, M. K.; Diau, E. W. G.; Yeh, C. Y.; Zakeeruddin, S. M.; Gratzel, M., Porphyrin-Sensitized Solar Cells

with Cobalt (II/III)-Based Redox Electrolyte Exceed 12 Percent Efficiency. Science 2011, 334 (6056), 629-634.

[106] Chen, X.; Mao, S. S., Titanium dioxide nanomaterials: Synthesis, properties, modifications, and applications. Chem. Rev. 2007, 107 (7), 2891-2959.

[107] Li, W.; Wu, Z. X.; Wang, J. X.; Elzatahry, A. A.; Zhao, D. Y., A Perspective on Mesoporous TiO2 Materials. Chem. Mat. 2014, 26 (1), 287-298.

[108] Wold, A., PHOTOCATALYTIC PROPERTIES OF TIO2. Chem. Mat. 1993, 5 (3), 280-283.

[109] Wu, H. B.; Hng, H. H.; Lou, X. W., Direct Synthesis of Anatase TiO2 Nanowires with Enhanced Photocatalytic Activity. Adv. Mater. 2012, 24 (19), 2567-2571.

[110] Pu, X.; Song, W. X.; Liu, M. M.; Sun, C. W.; Du, C. H.; Jiang, C. Y.; Huang, X.; Zou, D. C.; Hu, W. G.; Wang, Z. L., Wearable Power-Textiles by Integrating Fabric Triboelectric Nanogenerators and Fiber-Shaped Dye-Sensitized Solar Cells. Adv. Energy Mater. 2016, 6 (20), 9.

[111] Liu, G. C.; Wang, M. X.; Wang, H.; Ardhi, R. E. A.; Yu, H. J.; Zou, D. C.; Lee, J. K., Hierarchically structured photoanode with enhanced charge collection and light harvesting abilities for fiber-shaped dye-sensitized solar cells. Nano Energy 2018, 49, 95-102.

[112] Liu, G. C.; Wang, H.; Wang, M. X.; Liu, W. B.; Ardhi, R. E. A.; Zou, D. C.; Lee, J. K., Study on a stretchable, fiber-shaped, and TiO2 nanowire array-based dye-sensitized solar cell with electrochemical impedance spectroscopy method. Electrochim. Acta 2018, 267, 34-40.

[113] Li, Z. D.; Zhou, Y.; Yang, Y. H.; Dai, H., Electrophoretic deposition of graphene-TiO2 hierarchical spheres onto Ti thread for flexible fiber-shaped dye-sensitized solar cells. Mater. Des. 2016, 105, 352-358.

[114] Peng, M.; Yan, K.; Hu, H. W.; Shen, D. H.; Song, W. X.; Zou, D. C., Efficient fiber shaped zinc bromide batteries and dye sensitized solar cells for flexible power sources. J. Mater. Chem. C 2015, 3 (10), 2157-2165.

[115] Peng, M.; Dong, B.; Cai, X.; Wang, W.; Jiang, X. M.; Wang, Y. H.; Yang, Y.; Zou, D. C., Organic dye-sensitized photovoltaic fibers. Sol. Energy 2017, 150, 161-165.

[116] Wen, Z.; Yeh, M. H.; Guo, H. Y.; Wang, J.; Zi, Y. L.; Xu, W. D.; Deng, J. N.; Zhu, L.; Wang, X.; Hu, C. G.; Zhu, L. P.; Sun, X. H.; Wang, Z. L., Self-powered textile for wearable electronics by hybridizing fiber-shaped nanogenerators, solar cells, and supercapacitors. Sci. Adv. 2016, 2 (10), 8.

[117] Fu, X. M.; Sun, H.; Xie, S. L.; Zhang, J.; Pan, Z. Y.; Liao, M.; Xu, L. M.; Li, Z.; Wang, B. J.; Sun, X. M.; Peng, H. S., A fiber-shaped solar cell showing a record power conversion efficiency of 10%. J. Mater. Chem. A 2018, 6 (1), 45-51.

[118] Liu, G. C.; Peng, M.; Song, W. X.; Wang, H.; Zou, D. C., An 8.07% efficient fiber dye-sensitized solar cell based on a TiO2 micron-core array and multilayer structure photoanode. Nano Energy 2015, 11, 341-347.

[119] Lv, Z. B.; Yu, J. F.; Wu, H. W.; Shang, J.; Wang, D.; Hou, S. C.; Fu, Y. P.; Wu, K.; Zou, D. C., Highly efficient and completely flexible fiber-shaped dye-sensitized solar cell based on TiO2 nanotube array. Nanoscale 2012, 4 (4), 1248-1253.

[120] Liu, G. C.; Gao, X.; Wang, H.; Kim, A. Y.; Zhao, Z. X.; Lee, J. K.; Zou, D. C., A novel photoanode with high flexibility for fiber-shaped dye sensitized solar cells. J. Mater. Chem. A 2016, 4 (16), 5925-5931.

[121] Song, W. X.; Wang, H.; Liu, G. C.; Peng, M.; Zou, D. C., Improving the photovoltaic performance and flexibility of fiber-shaped dye-sensitized solar cells with atomic layer deposition. Nano Energy 2016, 19, 1-7.

[122] Tao, H.; Fang, G. J.; Ke, W. J.; Zeng, W.; Wang, J., In-situ synthesis of TiO2 network nanoporous structure on Ti wire substrate and its application in fiber dye sensitized solar cells. J. Power Sources 2014, 245, 59-65.

[123] Chen, L.; Zhou, Y.; Dai, H.; Yu, T.; Liu, J. G.; Zou, Z. G., One-step growth of CoNi2S4 nanoribbons on carbon fibers as platinum-free counter electrodes for fiber-shaped dye-sensitized solar cells with high performance: Polymorph-dependent conversion efficiency. Nano Energy 2015, 11, 697-703.

[124] Yang, Z. B.; Deng, J.; Sun, X. M.; Li, H. P.; Peng, H. S., Stretchable, Wearable Dye-Sensitized Solar Cells. Adv. Mater. 2014, 26 (17), 2643-2647.

[125] Chen, T.; Qiu, L. B.; Yang, Z. B.; Cai, Z. B.; Ren, J.; Li, H. P.; Lin, H. J.; Sun, X. M.; Peng, H. S., An Integrated "Energy Wire" for both Photoelectric Conversion and Energy Storage. Angew. Chem.-Int. Edit. 2012, 51 (48), 11977-11980.

[126] Ali, A.; Shah, S. M.; Bozar, S.; Kazici, M.; Keskin, B.; Kaleli, M.; Akyurekli, S.; Gunes, S., Metal-free polymer/MWCNT composite fiber as an efficient counter electrode in fiber shape dye-sensitized solar cells. Nanotechnology 2016, 27 (38), 10.

[127] Zhang, J. X.; Wang, Z. P.; Li, X. L.; Yang, J.; Song, C. H.; Li, Y. P.; Cheng, J. L.; Guan, Q.; Wang, B., Flexible Platinum-Free Fiber-Shaped Dye Sensitized Solar Cell with 10.28% Efficiency. ACS Appl. Energ. Mater. 2019, 2 (4), 2870-2877.

[128] Chen, X. X.; Tang, Q. W.; He, B. L.; Lin, L.; Yu, L. M., Platinum-Free Binary Co-Ni Alloy Counter Electrodes for Efficient Dye-Sensitized Solar Cells. Angew. Chem.-Int. Edit. 2014, 53 (40), 10799-10803.

[129] Dinari, M.; Momeni, M. M.; Goudarzirad, M., Dye-sensitized solar cells based on nanocomposite of polyaniline/graphene quantum dots. J. Mater. Sci. 2016, 51 (6), 2964-2971.

[130] Zhuo, J. Q.; Caban-Acevedo, M.; Liang, H. F.; Samad, L.; Ding, Q.; Fu, Y. P.; Li, M. X.; Jin, S., High-Performance Electrocatalysis for Hydrogen Evolution Reaction Using Se-Doped Pyrite-Phase Nickel Diphosphide Nanostructures. ACS Catal. 2015, 5 (11), 6355-6361.

[131] Chen, H. C.; Jiang, J. J.; Zhao, Y. D.; Zhang, L.; Guo, D. Q.; Xia, D. D., One-pot synthesis of porous nickel cobalt sulphides: tuning the composition for superior pseudocapacitance. J. Mater. Chem. A 2015, 3 (1), 428-437.

[132] Gao, M. R.; Lin, Z. Y.; Zhuang, T. T.; Jiang, J.; Xu, Y. F.; Zheng, Y. R.; Yu, S. H., Mixed-solution synthesis of sea urchin-like NiSe nanofiber assemblies as economical Pt-free catalysts for electrochemical H-2 production. J. Mater. Chem. 2012, 22 (27), 13662-13668.

[133] Shao, L.; Qian, X.; Li, H. M.; Xu, C.; Hou, L. X., Shape-controllable syntheses of ternary Ni-Co-Se alloy hollow microspheres as highly efficient catalytic materials for dye-sensitized solar cells. Chem. Eng. J. 2017, 315, 562-572.

[134] Chen, L.; Zhou, Y.; Dai, H.; Li, Z.; Yu, T.; Liu, J.; Zou, Z., Fiber dye-sensitized solar cells consisting of TiO 2 nanowires arrays on Ti thread as photoanodes through a low-cost, scalable route. Journal of Materials Chemistry A 2013, 1 (38), 11790-11794.

[135] Theerthagiri, J.; Senthil, R.; Buraidah, M.; Raghavender, M.; Madhavan, J.; Arof, A., Synthesis and characterization of (Ni1− xCox) Se2 based ternary selenides as electrocatalyst for triiodide reduction in dye-sensitized solar cells. Journal of Solid State Chemistry 2016, 238, 113-120.

[136] Zhu, Y.; Ji, X.; Wu, Z.; Liu, Y., NiCo2S4 hollow microsphere decorated by acetylene black for high-performance asymmetric supercapacitor. Electrochimica Acta 2015, 186, 562-571.

[137] Peng, S.; Li, L.; Tan, H.; Cai, R.; Shi, W.; Li, C.; Mhaisalkar, S. G.; Srinivasan, M.; Ramakrishna, S.; Yan, Q., MS2 (M= Co and Ni) Hollow Spheres with Tunable Interiors for High-Performance Supercapacitors and Photovoltaics. Advanced Functional Materials 2014, 24 (15), 2155-2162.

[138] Shi, W.; Zhang, X.; Che, G., Hydrothermal synthesis and electrochemical hydrogen storage performance of porous hollow NiSe nanospheres. International journal of hydrogen energy 2013, 38 (17), 7037-7045.

[139] Shen, L.; Yu, L.; Wu, H. B.; Yu, X.-Y.; Zhang, X.; Lou, X. W. D., Formation of nickel cobalt sulfide ball-in-ball hollow spheres with enhanced electrochemical pseudocapacitive properties. Nature communications 2015, 6 (1), 1-8.

[140] Yu, X. L.; Cao, C. B.; Zhu, H. S.; Li, Q. S.; Liu, C. L.; Gong, Q. H., Nanometer-Sized Copper Sulfide Hollow Spheres with Strong Optical-Limiting Properties. Advanced Functional Materials 2007, 17 (8), 1397-1401.

[141] Zhang, G.; Wang, W.; Yu, Q.; Li, X., Facile one-pot synthesis of PbSe and NiSe2 hollow spheres: Kirkendall-effect-induced growth and related properties. Chemistry of Materials 2009, 21 (5), 969-974.

BIOGRAPHICAL SKETCH

Brishty Deb Choudhury started her Master's program at the University of Texas Rio Grande Valley in 2018. She received her Bachelor's of Science degree (2015) in Chemical Engineering from the Shahjalal University of Science and Technology, Bangladesh. She worked as a research assistant at the Photonics and Energy Research Laboratory under Dr. Mohammed Uddin during her Master's studies. She received her Master's of Science degree in Chemistry in August of 2020. She can be reached at: brishtychoudhury@gmail.com